On the Structure and Dynamics of Monthly Mean Sea Level Anomalies along the Pacific Coast of North and South America

D. B. ENFIELD AND J. S. ALLEN

School of Oceanography, Oregon State University, Corvallis 97331

(Manuscript received 6 August 1979, in final form 18 December 1979)

ABSTRACT

The behavior and relationship of anomalies of monthly mean sea level, coastal sea surface temperature and alongshore wind stress for the eastern Pacific Ocean during the period 1950–74 have been studied. Sea level and temperature records from Yakutat, Alaska (59°N) to Valparaiso, Chile (33°S) and computed alongshore wind stress at near coastal grid points from Yakutat to Matzatlan, Mexico (23°N) have been utilized. The positive and negative sea level anomalies, corresponding to El Niño-anti El Niño cycles, are well correlated throughout the tropics of both hemispheres and are detectable at the California stations. From Crescent City to Antofagasta, Chile the sea level anomalies were correlated with the Southern Oscillation Index above the 99% significance level. The maximum station separations for which sea level anomalies were correlated among themselves above the 99% significance level varied from 6000 km (Yakutat to San Diego) to more than 12 000 km (Prince Rupert to Matarani). A well-defined lagged correlation structure of the sea level anomalies exists which suggests a poleward propagation of events in the Northern Hemisphere and leads to a phase speed estimate of 180 ± 100 km day^{-1}. Cross-spectral results imply that the propagation occurs predominantly at subannual frequencies and lead to a lower range of phase speeds (60–100 km day^{-1}). These estimates are consistent with theory and observations concerning wave propagation processes but are too fast to be explained by large-scale advective processes. The correlations of sea level anomalies with anomalies of the local alongshore wind stress are greatest from Sitka to Crescent City; they decrease south of Crescent City, with a marginal value at San Francisco and no significant correlation at San Diego. Between Neah Bay and San Francisco, the relation between the alongshore sea level slope and the alongshore component of the wind stress is consistent with a mass balance between a geostrophic onshore-offshore velocity below the surface layer and an onshore-offshore Ekman transport.

1. Introduction

During El Niño occurrences there is an abrupt rise in sea level in the eastern equatorial Pacific, coincident with a sea level fall in the western Pacific (e.g. Wyrtki, 1977). To explain this, Wyrtki (1975) proposed that interannual, mid-equatorial Pacific trade wind anomalies cause the accumulation of upper layer water in the west (strong trades) and its subsequent tendency to return eastward (weak trades) in the form of an equatorially trapped internal Kelvin wave. McCreary (1976) confirmed analytically the importance of equatorial zonal wind changes in producing eastward propagating Kelvin waves along the equator in association with El Niño. The abruptness of the sea level rise and thermocline depression in the eastern Pacific were reproduced numerically by Hurlburt *et al.* (1976), again in conjunction with Kelvin waves excited by wind changes. Moore (1968) had shown theoretically that equatorial disturbances incident on the eastern boundary may be partially transmitted poleward as coastal trapped Kelvin waves. This feature was also reproduced in the analysis of Hurlburt *et al.* (1976).

The notion that interannual disturbances in sea level of a wavelike nature propagate poleward from the equator along the eastern boundary has not been tested against observations. Roden (1966) found significant alongshore coherence in monthly sea level anomalies along the Pacific coast of North America for scales of up to 1200 km and frequencies of 0–6 cycles per year (cpy). But his study did not relate these fluctuations to sea level anomalies farther south or to El Niño occurrences. Bretschneider and McLain (1976) noted considerable visual similarity in monthly sea level anomalies from Chile to as far north as Adak, Alaska, but no quantitative attempt was made to determine the effective poleward penetration of the El Niño-related anomalies. Thus, the large-scale, alongshore structure of sea level anomalies along the eastern boundary, their relation to the El Niño, and the mechanism(s) for their coherence have yet to be established.

Over much of the Pacific coast of North America

0022-3670/80/040557-22$09.50

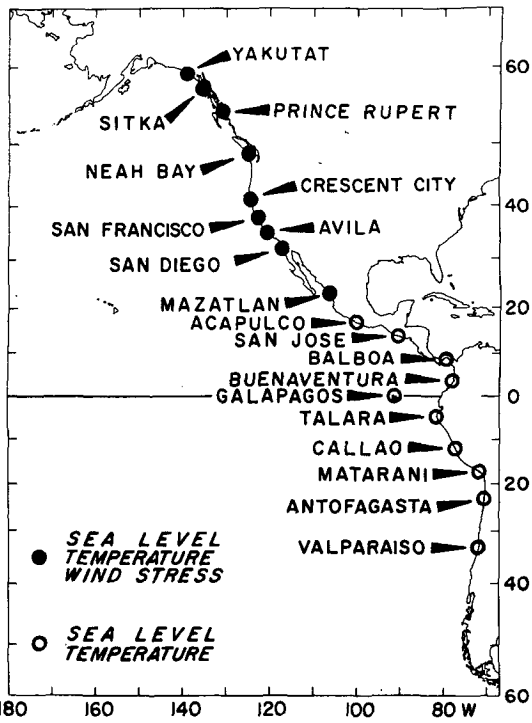

FIG. 1. Locations of sea level stations. Sea level and temperature data were used for all stations. Wind stress was used only for FNWC grid points near North American stations (closed circles).

(38–49°N) sea level responds well to fluctuations in the local alongshore wind stress at periods of two days to several weeks (Smith, 1974; Huyer *et al.*, 1975; Osmer and Huyer, 1978). It would be of interest to know 1) to what extent these results extend to the variability at greater time and distance scales, 2) whether or not a poleward increase in sea level response to local winds accompanies a poleward damping of the equatorial signal in sea level, and 3) if the observed sea level-wind stress relationship can be explained through simple dynamical arguments.

In this study we examine the alongshore structure of monthly sea level anomalies from Alaska to Chile, and their relationships with coastal temperature and alongshore wind stress anomalies. The interannual variability of sea level associated with El Niño occurrences, and its meridional integrity, are of particular interest. The possibility of a wave propagative coherence mechanism is examined as well as alternative connective modes. We examine the meridional change in the anomalous sea level response to alongshore wind stress along the Pacific coast of North America, as well as its consistency with a simple dynamical model involving geostrophy and Ekman transport.

2. Data

We obtained monthly mean sea levels for Pacific coastal and island stations from the NORPAX data bank as they were originally processed by K. Wyrtki. The important criteria in the selection of sea level stations for analysis were 1) geographic coverage of a large latitude range along the Pacific eastern boundary, 2) minimization of nonuniformities in station spacing, 3) maximum time coverage of a common period of sufficient length (~25 years), 4) existence of intervening stations (not to be analyzed) for data quality checks and patching of record gaps, and 5) avoidance of tide stations having poor exposure to oceanic effects. Fig. 1 shows the sea level stations selected for analysis (see also Table 1). The latitude range is limited by the Alaskan mainland in the north and by insufficient data in the south (southern Chile). The average station separation is ~1000 km. The larger separations south of Prince Rupert, Neah Bay, San Diego and San Jose are due to the lack of data or the need to preserve independent time series for patching purposes. We selected the 25-year (300-month) period from 1950–74 for analysis. This period is covered completely by 13 of the 19 stations. Of the remaining six stations, five cover at least 20 years and the Galapagos station covers 15 years. The exposure of North American Pacific tide stations is discussed by Roden (1960); those located on rivers and straits were not selected for this study. The Central and South American stations selected are located in harbors or on the open coast.

The individual sea level time series were separated into their average annual variations and the anomalies from these by taking out the long-term mean, calculating the mean value for each of the 12 months of the year to form the average annual cycle, and finally subtracting the annual cycle from the time series to form the anomalies. Gaps in the anomaly time series were filled by regressing values from a several year period spanning the gap on data from the same period at a neighboring station not chosen for analysis. Linear trends in the corrected and patched time series of anomalies were removed.

A. Bakun (Pacific Environmental Group, National Marine Fisheries Service, Monterey) provided the monthly averaged north and east components of wind stress calculated from monthly mean atmospheric pressure fields prepared by Fleet Numerical Weather Central (FNWC) for nine points near tide stations from Yakutat to Mazatlan (see Table 1). The analyses and some of the characteristics of this data set are described by Bakun (1973, 1975). Due to considerations of tropical ageostrophy and inadequacies in the FNWC grid analysis at low latitudes (Bakun, personal communication), we did

TABLE 1. Locations of measurement stations and data sources for sea level, sea level atmospheric pressure, shore temperature and wind stress. All sea level data were obtained from the NORPAX Data Bank (Scripps Institute of Oceanography, La Jolla). Wind stress data were obtained from Fleet Numerical Weather Central (FNWC, Monterey). Other sources are: National Center for Atmospheric Research (NCAR); National Ocean Survey (NOS); Environment Canada (EC); Panama Canal Co. (PCC); Instituto Oceanografico de la Armada (INOCAR); Corporacion Peruana de Aviacion Civil (CORPAC); and Direccion de Hidrografia y Navegacion de la Marina (DHNM). The station abbreviations given in the third column are used in other figures and tables to identify the stations listed here.

Sea level				Pressure		Shore temperature		Wind stress	
Station	Country	Symbol	Latitude	Station	Source	Station	Source	Latitude (°N)	Longitude (°W)
Yakutat	U.S.	YA	59.5°N	Yakutat	NCAR	Yakutat	NOS	59	139
Sitka	U.S.	SI	57.0°N	Juneau	NCAR	Sitka	NOS	57	135
Prince Rupert	Canada	PR	54.3°N	Annette Is.	NCAR	Langara Is.	EC	54	130
Neah Bay	U.S.	NB	48.4°N	Quillayute	NCAR	Neah Bay	NOS	48	124
Crescent City	U.S.	CC	41.8°N	41°N, 124°W	FNWC	Crescent City	NOS	41	124
San Francisco	U.S.	SF	37.8°N	San Francisco	NCAR	San Francisco	NOS	37	122
Avila Beach	U.S.	AV	35.2°N	35°N, 120°W	FNWC	Avila	NOS	35	120
San Diego	U.S.	SD	32.7°N	San Diego	NCAR	La Jolla	NOS	32	117
Mazatlan	Mexico	MZ	23.2°N	23°N, 106°W	FNWC	Mazatlan	NOS	23	106
Acapulco	Mexico	AC	16.8°N	16°N, 100°W	FNWC	Acapulco	NOS		
San Jose	Guatemala	SJ	13.9°N	14°N, 90°W	FNWC	San Jose	NOS		
Balboa (C.Z.)	Panama	BA	9.0°N	9°N, 79°W	FNWC	Balboa	PCC		
Buenaventura	Colombia	BV	3.9°N	4°N, 77°W	FNWC	Buenaventura	NOS		
Galapagos Is.	Ecuador	GA	0.5°S	—	—	Galapagos Is.	INOCAR		
Talara	Peru	TA	4.6°S	Talara	CORPAC	Talara	DHNM		
Callao	Peru	CA	12.0°S	Lima	CORPAC	Callao	DHNM		
Matarani	Peru	MA	17.0°S	Tacna	CORPAC	Matarani	DHNM		
Antofagasta	Chile	AN	23.6°S	Antofagasta	NCAR	Antofagasta	NOS		
Valparaiso	Chile	VA	33.0°S	Valparaiso	NCAR	Valparaiso	NOS		

not attempt to utilize geostrophic stresses south of Mazatlan. It should also be mentioned that these stress values may be relatively less accurate off southern California since, as Bakun (1973) has pointed out, in the summer the effect of the coastal mountain range in that region is likely to cause an overestimation of the stress. The alongshore component of the wind stress at each grid point was calculated based on the general orientation of the local continental margin, as indicated by the 200 m isobath (Table 2).

Time series of monthly averaged shore temperature and sea level atmospheric pressure were obtained for locations at or near the tide stations from the sources summarized in Table 1. For stations from Mazatlan to Buenaventura, grid point pressures from the FNWC pressure analyses were used after being "calibrated" by regression to agree with incomplete station pressures. Otherwise, the shore temperature and pressure data were processed in the same manner as for sea level.

To make water elevations representative of the total pressure just below the sea surface, the sea level (cm) was adjusted by adding the equivalent of the atmospheric pressure in centimeters of water. This was done before separating the data into annual and anomalous components. The sea level data at Baltra Island (Galapagos) was not adjusted due to the non-availability of pressure data. The higher correlations at low latitudes between adjusted and unadjusted sea level anomalies (Table 2) indicate that the adjustment for atmospheric pressure is of little significance at tropical stations, where pressure fluctuations are small.

3. Comparative behavior of anomalies, average annual cycles and long-term means

It is instructive to examine some characteristics of the long-term means and average annual cycles and to compare their structures and relationships to those of the anomalies.

The summary statistics for the data are given in Table 2 for the period 1950–74. Two of the features seen are 1) the monotonic poleward decrease of mean shore temperatures and 2) the north-to-south transition from poleward to equatorward direction of the mean alongshore wind stress off North America. Fig. 2 shows latitudinal profiles of anomaly variance, total variance and their ratio for sea level, shore temperature and alongshore wind stress. Additional features seen are 3) a monotonic decrease in the stress variance (anomaly and seasonal) from Yakutat to Neah Bay, and uniform variance

TABLE 2. Record lengths (n), means and standard deviations (sd) of monthly averaged data (t) and anomalies (a). Also given are the correlation coefficients (r) between the adjusted and unadjusted sea level anomalies, and the angles clockwise from true north assumed as the isobath orientation in computing wind stress components.

Station	Adjusted sea level (cm)			Pressure (mb)		Shore temperature (°C)				Alongshore stress (dyn cm^{-2})				
	n	sd(t)	sd(a)	sd(a)	r	n	mean	sd(t)	sd(a)	n	mean	sd(t)	sd(a)	angle
YA	300	7.5	4.8	4.5	0.906	300	7.5	3.6	0.9	300	1.17	1.65	0.97	305
SI	300	7.6	4.5	3.8	0.937	300	8.4	3.6	0.8	300	0.94	1.20	0.71	330
PR	300	7.4	5.1	3.5	0.948	300	8.5	2.2	0.7	300	0.72	1.09	0.67	325
NB	300	10.5	5.6	3.2	0.983	300	9.7	1.9	0.8	300	0.26	0.64	0.37	345
CC	300	8.2	4.8	2.5	0.958	296	11.7	1.9	1.0	300	−0.32	0.74	0.38	345
SF	300	6.5	4.3	2.0	0.914	300	12.9	1.9	0.8	300	−0.68	0.76	0.37	330
AV	300	6.4	4.3	1.4	0.909	300	13.9	1.6	0.9	300	−1.00	0.85	0.39	340
SD	300	5.8	3.6	1.2	0.933	300	16.7	2.4	0.8	300	−1.04	0.85	0.37	340
MZ	264	10.8	6.0	1.0	0.990	241	25.5	3.7	1.2	300	−0.28	0.52	0.33	320
AC	300	8.6	6.3	0.9	0.990	271	28.0	1.6	0.9					
SJ	240	7.8	6.6	1.0	0.990	252	29.4	0.8	0.6					
BA	300	10.2	4.8	0.7	0.998	300	27.0	1.6	0.8					
BV	240	7.7	4.7	0.6	0.992	249	28.1	0.6	0.5					
GA	182	6.1*	5.8*	—	—	182	23.4	2.1	1.3					
TA	300	5.4	4.9	0.7	0.986	300	19.1	2.1	1.5					
CA	300	5.0	4.4	0.7	0.969	300	16.7	1.7	1.4					
MA	300	4.5	4.1	0.9	0.947	273	14.3	2.2	1.0					
AN	252	3.9	3.5	1.3	0.909	240	17.3	2.1	0.6					
VA	252	4.4	3.5	1.3	0.898	240	13.9	1.4	0.7					

* Unadjusted (no pressure data obtained).

farther south; 4) the lack of marked latitudinal structure in the variability of sea level and temperature anomalies as opposed to the large station to station changes in the variance contribution of the annual cycles; and 5) the greater proportion of anomaly variance for shore temperature and sea level in the tropics as compared to middle and high latitudes. In the case of temperature this is mainly due to the high anomaly variance at the Galapagos Islands and Peru coastal stations; in the case of sea level, however, it is due to the small seasonal contribution at stations south of the equator.

Fig. 3 shows the departures of the average annual cycles of alongshore wind stress, sea level and shore temperature from the long-term means, arranged latitudinally for the selected stations. Positive values indicate relatively poleward wind stress, high sea level and warm temperature.

The poleward propagation of the annual cycle in wind stress off North America (Fig. 3, top) is due to the corresponding annual migrations and intensity changes of the semipermanent high and low pressure regions of the North Pacific. The shift of the coastal upwelling season from spring to midsummer with increasing latitude is a well-known consequence of this (Bakun, 1973). Off the Oregon coast, the annual cycles in the alongshore components of the wind stress and currents on the continental shelf, and coastal sea level are similar (Huyer *et al.*, 1979), reflecting the effect of seasonal wind variability on the nearshore flow. Such a similarity can be seen in Fig. 3 (top, middle), but close inspection reveals that at most stations the sea level minimum occurs 1–2 months before the equatorward wind stress maximum. Reid and Mantyla (1976) point out that the winter rise of coastal sea level is out of phase with the general mid-ocean cycle of steric elevations caused by the annual insolation extremes (represented by shore temperatures in Fig. 3, bottom). When they subtract the seasonal offshore steric levels from the annual cycles of coastal sea level, the adjusted curves reach minimum elevations 1–2 months later, more nearly in agreement with the wind stress. Another explanation for sea level leading the stress may be the influence of offshore circulations, such as the California Current (Hickey, 1979) and the Alaskan Gyre (Hayes and Schumacher, 1976; Hayes, 1979). Thus, the studies done to date indicate that the seasonal oscillation of coastal sea level is primarily due to the change in the strength of the nearshore circulation, modified by the annual insolation cycle and offshore flows.

Along Central America the lowest sea levels occur during January through May when the northeast trades reach their greatest intensity and southward displacement. This association is most evident at Balboa and is attributed to upwelling cycles induced by the monsoonal trade wind fluctuations in the Panama Bight (Forsbergh, 1969). Off South America the period of lowest sea level occurs in July–December, this time in conjunction with the maximum intensity in the southeast trades.

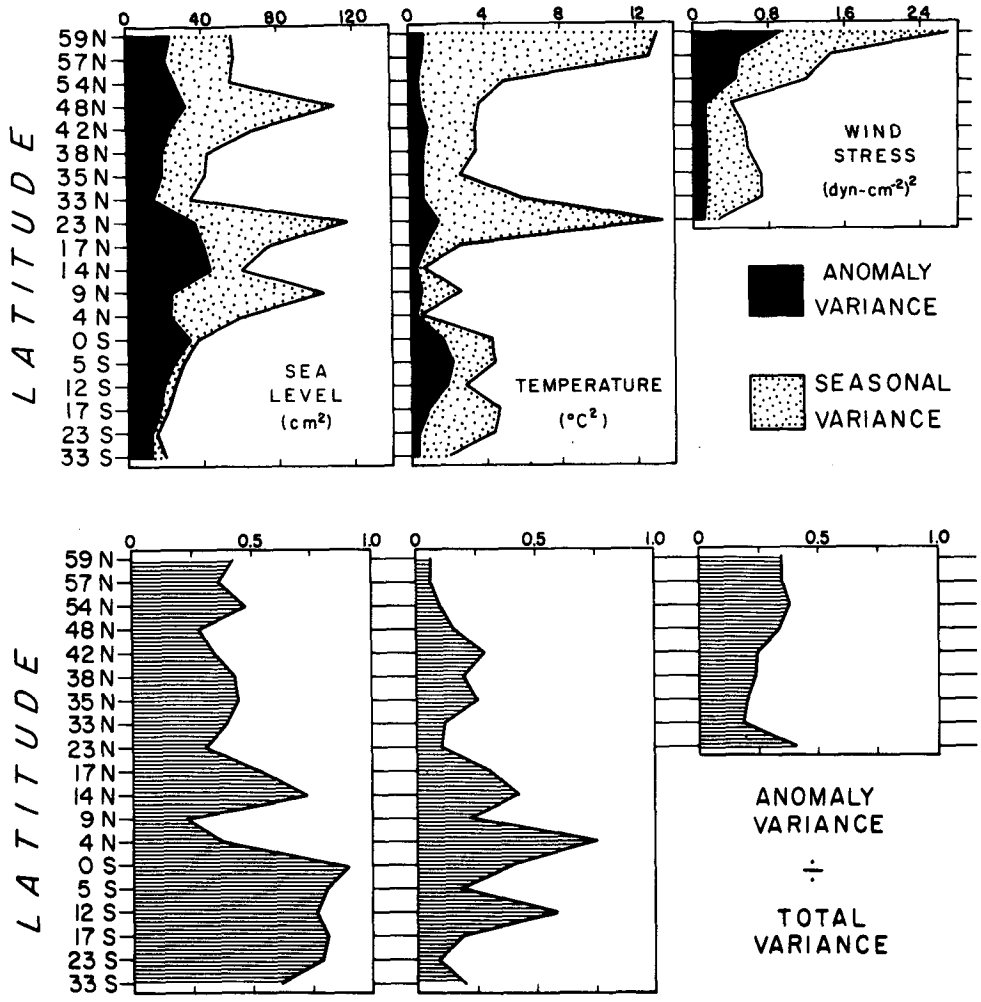

FIG. 2. Top: latitudinal distribution of anomaly variance (shaded black) and total variance (solid line) for sea level, shore temperature and alongshore wind stress. Bottom: latitudinal distribution of the ratio of anomaly to total variance (shaded) for the same variables (left to right).

As off North America, there is a slight tendency for this season to occur later at higher latitudes (off Chile).

Along the Pacific coast of North America the annual variation of shore temperature (Fig. 3, bottom) reflects neither the phase shift nor the lower values in the spring–summer that would indicate a coupling with the alongshore wind (such as has been observed for the vertical density profiles over the Oregon shelf (Huyer, 1977)). Instead, temperatures are uniformly warmest in July–August, in phase with the solar heating cycle. Something similar occurs for the South American coast. The Chilean stations experience the coldest shore temperatures in July–August, two months before sea level reaches a minimum. Along the Peru coast the cycles of sea level and shore temperature are in phase, as are the solar heating and the southeast trades. Therefore, the annual cycle of shore temperature is generally consistent with the local (solar) heating cycle, even where the latter is out of phase with stress-induced shelf processes.

4. Latitudinal structures of anomalies

The alongshore structures of anomalies were examined separately for sea level, shore temperature and alongshore wind stress by several methods: visual correlation of time series (Figs. 4a–c), autocorrelations and integral time scales (Figs. 5a and 5b; Table 3), lagged cross correlations (Figs. 6, 9 and 10) and cross spectra (Figs. 7 and 8).

We have used two statistical measures of integral time scales in our work. The one that characterizes the time scale $\bar{t}_1$ (or persistence) of a univariate process at a single location, $\{X(t)\}$, is the integral of its autocorrelation function over the lag (Lumley and Panofsky, 1964). For convenience in computa-

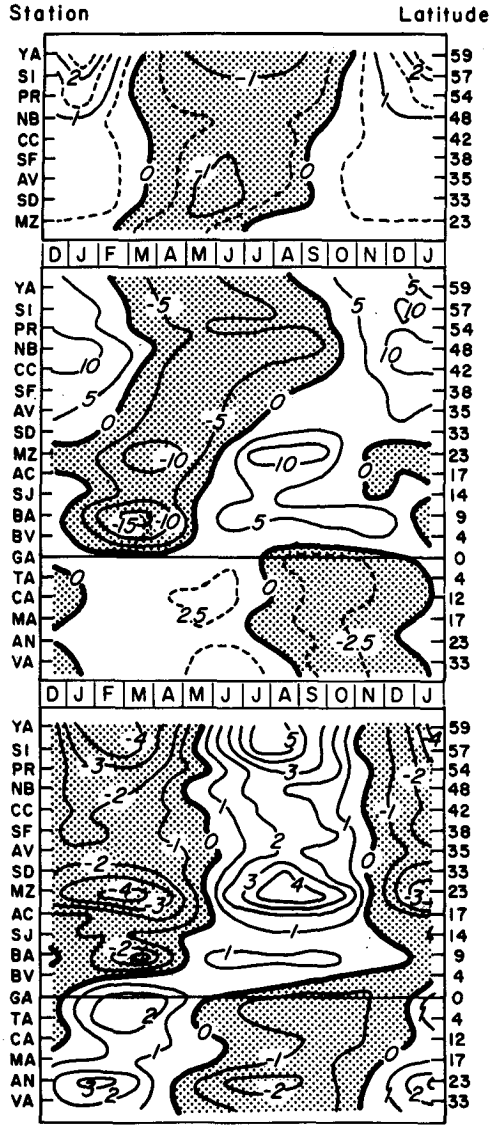

FIG. 3. Average annual variations of alongshore wind stress (top), sea level (middle) and shore temperature (bottom) by latitude, with the long-term mean values removed. Units are dyn cm^{-2} (stress), cm (sea level) and °C (temperature). Negative values are shaded.

tion, we redefine this time scale as the integral between zero lag and the lag at which the autocorrelation first becomes zero (τ_1), i.e.,

$$\tilde{t}_1 = \int_0^{\tau_1} C_x(\tau)d\tau. \qquad (4.1)$$

The integral time scales summarized in Table 3 were determined in this way. On the other hand, the time required to obtain two independent realizations of a *bivariate* process $\{X(t),Y(t)\}$ is assumed to be

$$\tilde{t}_2 = \int_{-\tau_2}^{\tau_2} C_x(\tau)C_y(\tau)d\tau \qquad (4.2)$$

(Davis, 1976). In practice, we integrated the autocorrelation products in (4.2) choosing τ_2 so that successive values of $\tilde{t}_2$ were essentially the same, a condition that was always satisfied at $\tau_2 = 10$ months. The equivalent degrees of freedom were computed by dividing the record length by $\tilde{t}_2$ and the significance levels of cross correlations (r) were then determined by referring to standard tables. The equivalent degrees of freedom varied from about one-third of the number of observations for cross correlations involving only sea level and temperature to about three-fourths for those involving only wind stress.

a. Sea level

The sea level anomalies are visually correlated over a large part of the latitude range examined

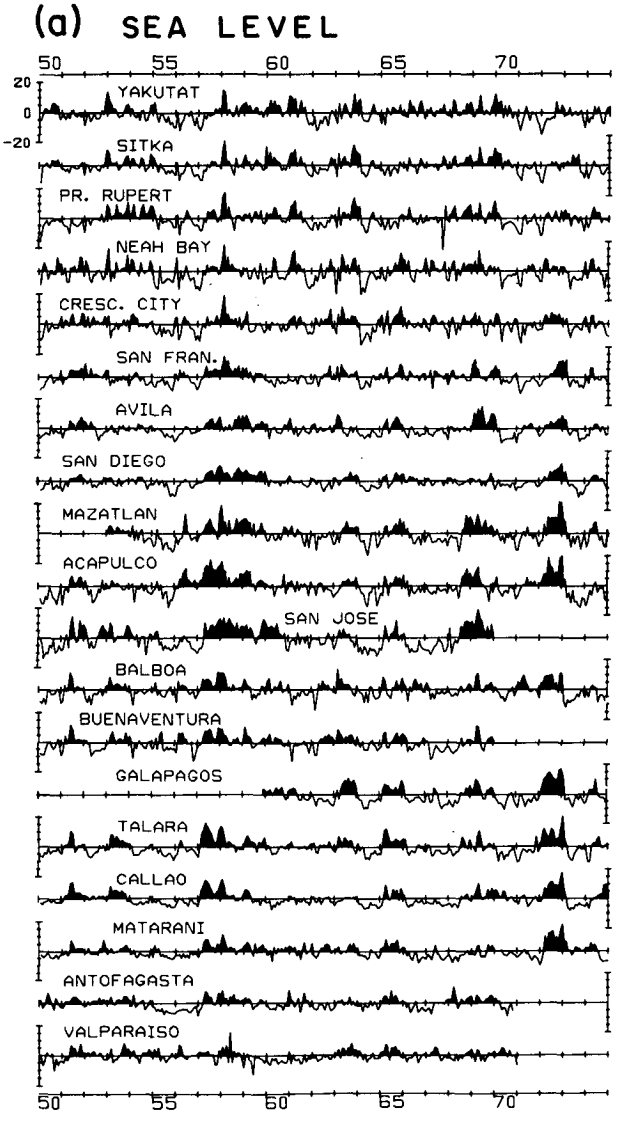

FIG. 4a. Time series of monthly anomalies of sea level from 1950 to 1974, inclusive. Positive anomalies are shaded black.

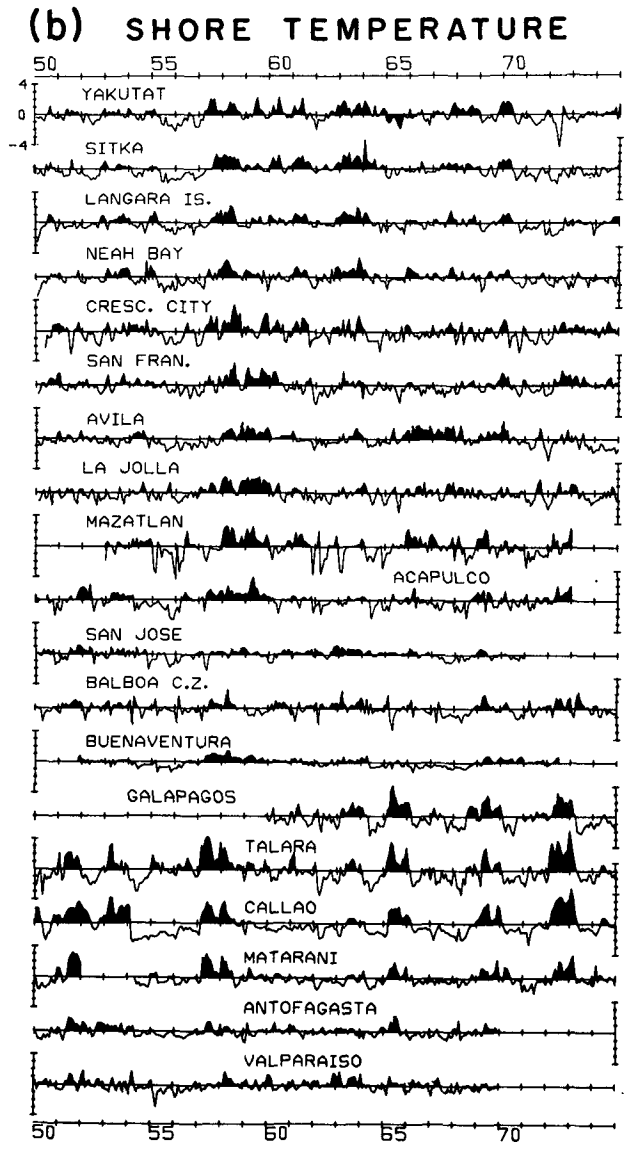

FIG. 4b. As in Fig. 4a except for shore temperatures.

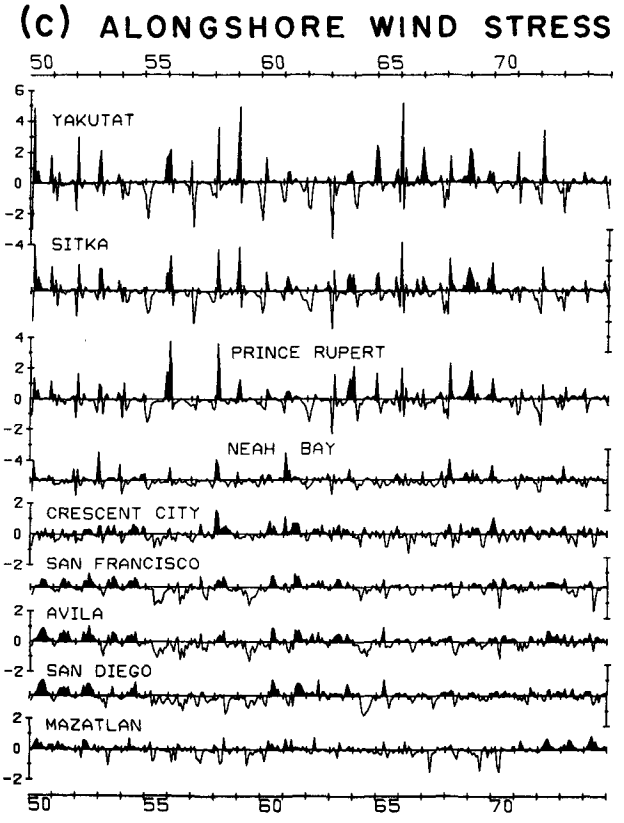

FIG. 4c. As in Fig. 4a except for alongshore wind stress.

(Fig. 4a). Interannual events of a year or longer appear to occur approximately simultaneously at most of the stations, especially those at low and midlatitudes, i.e., from Matarani to San Francisco. The El Niño (high sea level) events often cited in the literature (e.g., Quinn *et al.*, 1978) can be readily identified: 1951; 1953; 1957–58; 1963; 1965–66; 1969; and 1972–73. Shorter period fluctuations are visually coherent between neighboring stations or within regional groups (e.g., Crescent City to Yakutat, Galapagos to Matarani). The interannual fluctuations typical of El Niño are shown clearly at the four stations from Galapagos to Matarani where, in particular, a double peaked structure of the large El Niño events is evident. The anomaly signature from this "type region" can usually be traced south to Valparaiso and north to San Francisco or farther. The anomaly amplitudes decrease toward higher latitudes in the Southern Hemisphere and the equatorial signature usually becomes somewhat noisy north of San Francisco.

TABLE 3. Integral time scales in months for the anomalies of sea level, shore temperature and alongshore wind stress as determined by Eq. (4.1).

Station	Sea level	Temperature	Stress
YA	2.9	3.8	1.0
SI	2.7	6.5	1.0
PR	2.7	3.3	1.0
NB	1.8	3.3	1.1
CC	2.0	2.9	1.5
SF	3.2	3.9	1.9
AV	3.4	6.6	2.0
SD	3.9	4.5	2.0
MZ	3.7	2.9	2.3
AC	4.7	4.0	
SJ	5.2	3.2	
BA	2.4	2.3	
BV	2.5	8.1	
GA	3.6	3.3	
TA	3.4	3.6	
CA	3.9	5.1	
MA	3.6	3.6	
AN	4.2	2.9	
VA	2.8	3.3	

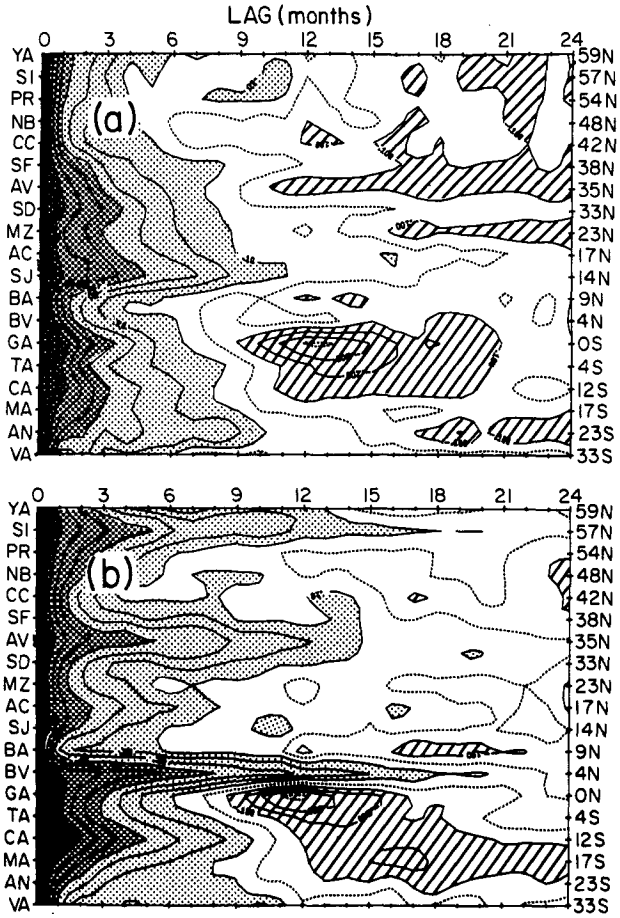

FIG. 5. Autocorrelation as a function of station (latitude) and lag for anomalies of (a) sea level and (b) shore temperature. Ranges of autocorrelation are indicated by diagonal lines for −0.1 to −0.4, light shading for 0.1 to 0.4, medium shading for 0.4 to 0.7 and dark shading for 0.7 to 1.0.

Fig. 5a is a contour plot of the autocorrelation of sea level as a function of latitude and lag. The corresponding time scales of Table 3 are the result of integrating each autocorrelation function out to the zero contour. Stations from San Francisco (38°N) to northern Chile (23°S) are characterized by broader autocorrelation functions and by time scales of 3–5 months, with the exceptions of Balboa (9°N) and Buenaventura (4°N). North of San Francisco and at Valparaiso, the time scales are less than 3 months. The greater persistence at low latitudes seems to reflect the relative importance of the interannual fluctuations in the tropics as opposed to shorter period wind related fluctuations at higher latitudes (Section 6). The interannual fluctuations are most important at the Galapagos Islands, Talara and Callao, which are characterized by relatively large negative autocorrelations at lags of about 10–20 months. Thus, at intervals of several years these stations experience relatively large and abrupt transitions from one extreme to another (as compared with other stations).

In Fig. 6a we adopt a contoured matrix format to show the distribution of maximum lagged cross-correlation between sea level records over all possible station pairs where 25 years of common record exist. All correlations were significant at the 95% level; less than 99% significance was obtained only between station pairs involving one of the two northernmost stations (Yakutat and Sitka) and one of the five southernmost (Acapulco, Balboa, Talara, Callao, Matarani). Neighboring stations (points close to the diagonal) were more highly correlated (0.52–0.82) and the greatest correlations occurred among the three northernmost stations (upper left).

For separations of 3000 km or less the correla-

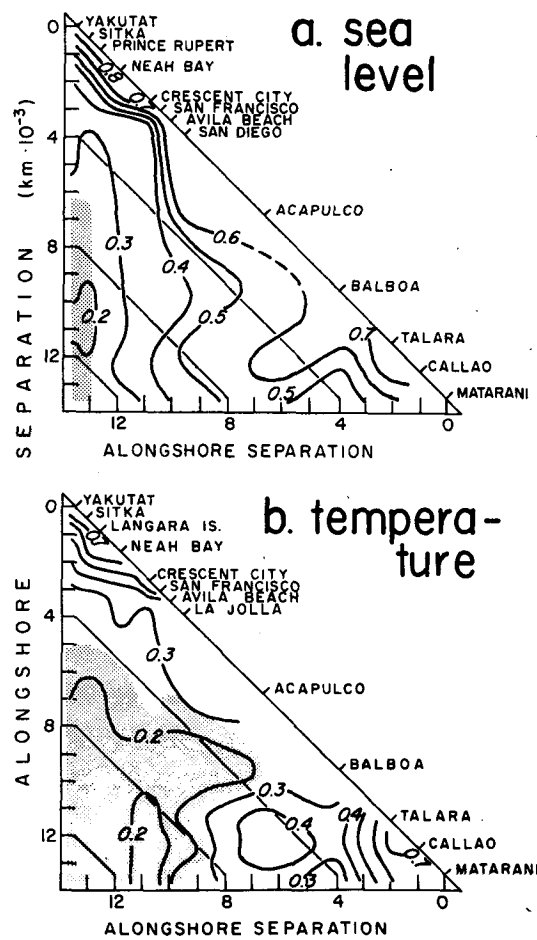

FIG. 6. Maximum lagged cross correlation of anomalies of (a) sea level and (b) shore temperature for station pairs where 25 years of sea level data exist. Distances (in thousands of kilometers) of the stations indicated on the diagonal from Yakutat and Matarani are given by the horizontal and vertical scales. The correlation for a pair of stations is found at the intersection of the vertical line through the northernmost station with the horizontal line through the southernmost one. Shading indicates correlation at less than 99% significance.

tion decreases with increasing separation (diagonally oriented contours). This suggests a separation-dependent coupling such as might occur due to anomalous regional wind forcing. At greater separations and south of San Francisco the contours tend to be more vertically oriented, indicating a tendency toward separation-independent behavior. These results are consistent with the spectral computations of Roden (1966), who calculated the areal coherence of sea level anomalies from Yakutat to San Diego for a frequency range of 0–6 cpy. For station pairs north of San Francisco the coherence decreases uniformly for all frequencies as the station separation increases. From San Francisco southward a similar coherence decay occurs at frequencies of 2–6 cpy, but at lower frequencies the coherence remains relatively high. Coherence scales of 1000–1500 km are indicated at the higher frequency range for all of the station pairs; but there appears to be a larger coherence scale at interannual frequencies, south of ~40°N.

To further investigate the coherence of interannual fluctuations at low latitudes as well as its change with increasing separation, we contoured the distribution of spectral coherence of anomalous sea level as a function of the alongshore distance between stations (Fig. 7). The plot is based on 78 coherence spectra from both hemispheres (15 degrees of freedom), obtained by crossing the record for each station equatorward of 40° latitude with those of all stations poleward of that station. Station pairs entirely north of 40°N were excluded because the interannual signal there is weak and would give low coherence at small separations. Sea level at stations separated by less than 2000 km tends to be significantly (95%) coherent at all frequencies except the annual (which was effectively removed). Only subannual frequencies are coherent beyond 2000 km, while only an interannual band, corresponding to periodicities of 2.5–4 years, is coherent beyond 4000 km. Hence the coherence scales of non-seasonal sea level are relatively short (2000–4000 km) for periodicities of 2 years or less, but large (up to 10 000 km) in the interannual band. This is consistent with the results of Roden (1966) and with the cross correlations already discussed (Fig. 6a). The high-frequency coherence at short separations is most likely due to the coupling effects of synoptic-scale atmospheric anomalies and/or regional ocean circulation effects.

That the interannual coherence of sea level is in fact associated with El Niño-related variability can be seen in Fig. 8 from the distribution of coherence between anomalous sea level and anomalies of the Southern Oscillation Index (SOI) as defined by Quinn (1974), *viz.*, the difference in sea level pressure between Easter Island (representative of the South Pacific high) and Darwin, Australia (representative of the Indonesian low). Quinn (1974) demonstrated the strong relationship between

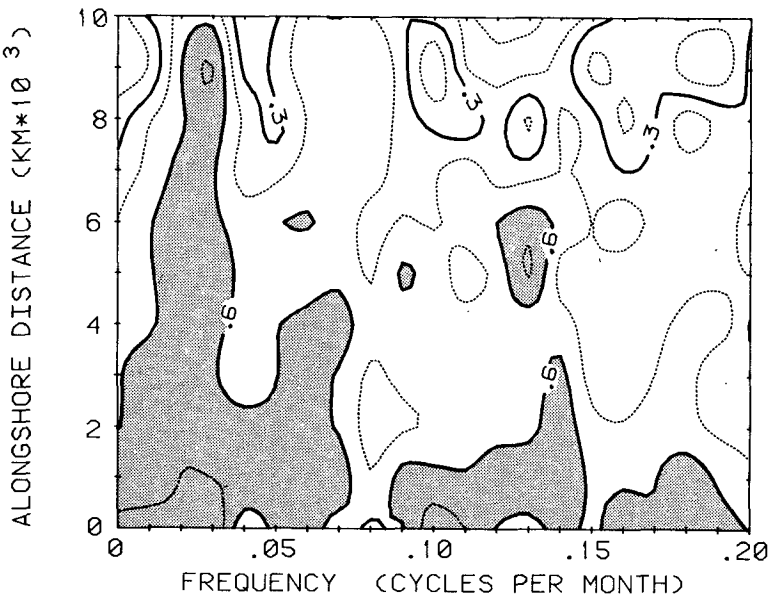

FIG. 7. Areal coherence of anomalous sea level as a function of the alongshore distance between stations. The plot is based on 78 coherence spectra from both hemispheres (15 degrees of freedom), obtained by crossing the record for each station equatorward of 40° latitude with those of all stations poleward of that station. Station pairs entirely north of 40°N were excluded. Shading indicates coherence at or above the 95% level.

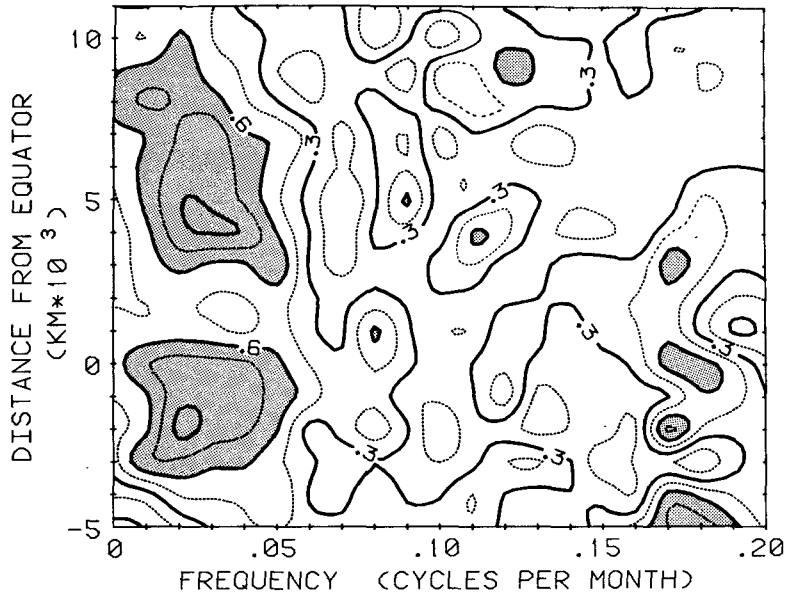

FIG. 8. Distribution of coherence between the Southern Oscillation Index (SOI) and the anomalies of sea level at 19 stations from Yakutat, Alaska (59°N) to Valparaiso, Chile (33°S). Positive ordinate values give the alongshore distance north of the equator, and shading indicates significance at or above the 95% level.

anomalously low SOI values and the occurrence of El Niño off of Peru and Ecuador. Along most of the Pacific coast of the Americas, sea level is significantly (95%) coherent with the SOI at interannual frequencies corresponding to periodicities of 2–5 years. Note that sea level at Balboa is less than 95% coherent with the SOI.

The low persistence of sea level anomalies at Balboa and Buenaventura (Fig. 5a; Table 3) and the low correlation of Balboa sea level anomalies with those of other stations (Fig. 6a) may be related to the anomalous behavior of the trade wind monsoon over the Panama Bight. Forsbergh (1969), in a review of the climatology of the Panama Bight, estimated that the mean latitude of the Intertropical Convergence Zone (ITCZ) across the Bight is ~8°N, or just south of Balboa. From December to April the ITCZ shifts southward and northerly winds prevail in the Gulf of Panama; from September to November the ITCZ is farther north and southwesterly winds prevail. During the northerly wind phase the northward flowing Colombia Current is weakened and sea levels at Balboa and Buenaventura are low. During the southwesterly wind phase the Colombia Current is stronger and sea levels are high. In a study of wind and sea surface temperature (SST) distributions in the western hemisphere, Hastenrath (1976) found that during years of high (low) SST in the eastern Pacific the ITCZ tended to be in a more southern (northern) position. This suggests an anomalous behavior of the trade winds that would tend to lower sea level in the Gulf of Panama during years characterized by high SST's. This would locally counteract the generally high sea level found in the eastern Pacific during anomalously warm years. Presumably, the effect is to modify the sea level anomalies at Balboa in such a way as to reduce their correlations with other sea level stations. This also might explain the low coherence of interannual sea level in the Panama Bight with the SOI (Fig. 8).

To illustrate the lag structure of sea level correlations we plotted the contours of correlation for all stations with Talara as a function of latitude and lag (Fig. 9a). Average values of the correlations corresponding to the 95 and 99% significance levels are 0.20 and 0.26, respectively. Talara is (95%) significantly correlated with stations from Valparaiso to the Gulf of Alaska. Maximum correlation occurs at zero lag from Valparaiso to Balboa. There is a well-defined ridge of maximum correlation extending northward from Balboa at an increasingly greater off-center displacement from the zero lag position, with Talara leading other stations. This well-defined lag structure is repeated for other pairings in the same sense, i.e., high-latitude stations lag low-latitude stations. As in the case of Talara, maximum correlations do not occur at lags greater than two months.[1]

[1] Yakutat correlated at 0.17, 0.14, 0.17 with Balboa for lags of one, two or three months, respectively and the 95% significance level was 0.16. The equivalent lag was assumed to be two months.

b. Shore temperature

The visual correlation between the time series of shore temperature (Fig. 4b) is considerably less than for sea level. The interannual variability associated with the El Niño is clear and coherent in the "type region" (Galapagos and Peru) and all of the major features from the sea level signature are reproduced there. However, only the high temperatures of 1957–58 are clearly traceable to all the Northern Hemisphere stations as well, and unlike the case of sea level, the onset of high temperatures of Mazatlan and California stations occurred nearly a year later than off Peru. Other Northern Hemisphere warm and cold periods disagree considerably with their Peru counterparts. The disagreement might in some instances be attributed to lag effects, e.g., the 1966–68 warm period at Mazatlan and southern California stations (cold in Peru) could be interpreted as a late-occurring manifestation of the 1965 warm period at the Peru stations.

The pattern of autocorrelation (Fig. 5b) and time scales (Table 3) for shore temperature exhibits both similarities and differences when compared to sea level. The most striking similarity is the occurrence of negative autocorrelations at the Galapagos Islands and Peru stations, beyond lags of about 10 months. Although the overall mean time scales are about the same for both sea level (3.3 months) and temperature (4.1 months), they are much less uniform for temperature. The distribution of maximum lagged cross correlations between temperature time series (Fig. 6b) also points to their greater individuality as compared with sea level. The cross correlations within the Peru region and within the area north of Crescent City are much higher than elsewhere. Correlations involving Avila (35°N) and Balboa (9°N) are low. Fewer cases were found for temperature than for sea level where the cross correlation exceeded the 99% level of significance. These fell into two geographic domains: north of Acapulco, where the cross correlation falls off rapidly with increasing station separation, and from Acapulco southward where correlations are less dependent on separation. The temperature anomalies within each of these two large regions were less correlated with those in the other than was true for sea level anomalies (as indicated by the larger shaded area).

The lag structure of temperature correlations is illustrated, as for sea level, by plotting contours of correlation for Talara with other stations (Fig. 9b). The 95 and 99% significance levels have average values of 0.21 and 0.27, respectively. As with sea level, the temperatures at higher latitudes lag those at Talara (except the Galapagos Islands and Antofagasta, which had maximum correlations at zero lag). Temperatures at Valparaiso, Avila and

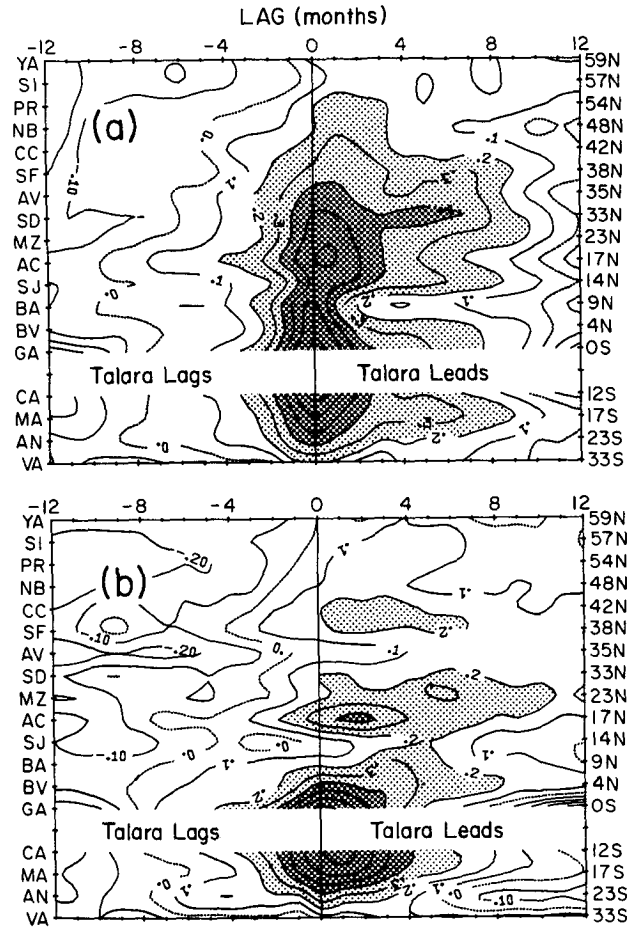

FIG. 9. Contours of lagged cross correlation between Talara and all other stations for (a) sea level and (b) shore temperature anomalies. Positive values from 0.2 (about 95% significance) to 0.4 have light shading; values > 0.4 have dark shading. Station abbreviations are defined in Table 1.

stations north of Crescent City are uncorrelated with the Talara temperatures at the 95% level. Maximum correlations for stations north of Buenaventura occur at lags of 2–8 months and no well-defined-ridge structure exists. The lags are largest at the North American stations, suggesting that the shore temperature anomalies there lag those at Peru stations by considerably more than is the case for sea level (Fig. 9a), although the significance of the correlations is marginal.

The markedly different lag structures of sea level and shore temperature anomalies suggests a lack of simultaneity between the two variables. The local, lagged correlation between sea level and shore temperature anomalies is shown in Fig. 10 as a function of station (latitude) and lag. The maximum correlation always occurs at zero lag and is significant at the 95% level or better. This seems inconsistent with the fact that large lags occur in tempera-

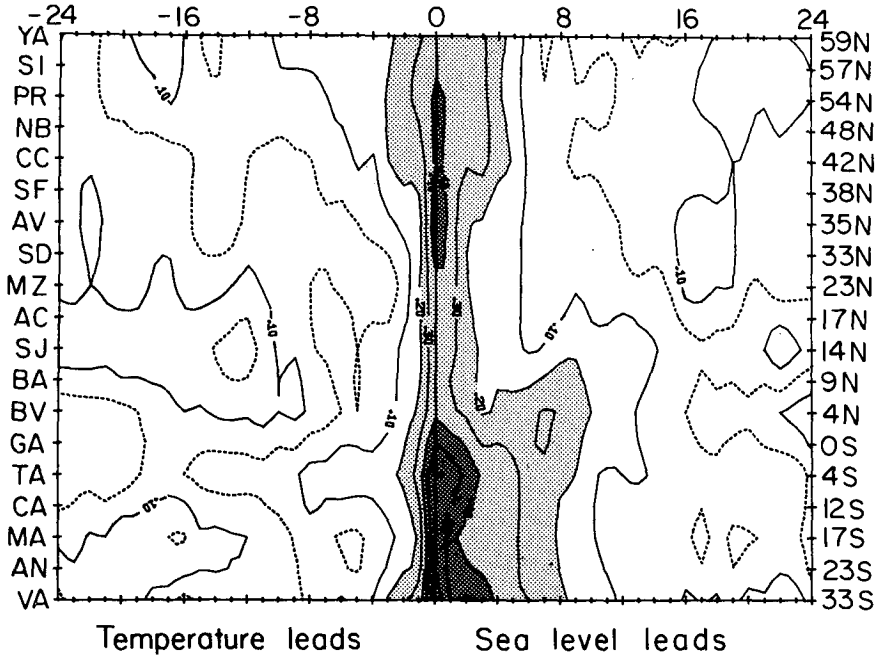

FIG. 10. Contours of maximum lagged cross correlation between sea level and shore temperature anomalies at each station. Light and dark shading indicate positive values from 0.2–0.4 and > 0.4, respectively.

ture between stations but not in sea level. It is therefore not clear from correlation analysis that non-simultaneity exists, or if it does, at which periodicities it may be most prominent. We therefore computed the first empirical orthogonal function (EOF) of the sea level and shore temperature anomalies in each of two regions: California (Crescent City to San Diego) and Peru (Talara to Matarani). We then did a cross-spectral analysis between the EOF's of sea level and temperature for each geographic group. In both regions the coherence between anomalies of sea level and shore temperature was greatest at frequencies of 0.5 cpy or less and the spectral densities in this band were an order of magnitude greater than at frequencies of 2 cpy or more. For the California EOF's the phase spectrum indicates that temperature lags sea level by 2–6 months at the interannual frequencies (0–0.5 cpy) but was nearly in phase (zero or one month) at higher frequencies. For the Peru EOF's temperature was nearly in phase (zero or one month) at all frequencies. The tendency for shore temperature anomalies to occur later at Northern Hemisphere midlatitude stations—as suggested by Figs. 4 and 9—and to lag sea level anomalies there by months, appears to be real and is limited to events on the interannual time scale.

In summary, sea level and shore temperature anomalies are both characterized by large variability on the interannual time scale associated with El Niño occurrences. Sea level is correlated over the entire latitude range studied. Over distances of several thousand kilometers or more, the areal correlation of sea level tends to be independent of station separation and due mainly to the low-frequency (interannual) variability, especially for stations south of 40°N. Sea level is also characterized by a well-defined lag structure wherein the mid- and high-latitude Northern Hemisphere stations consistently lag the tropical stations by 1–2 months. The temperature variability is areally correlated within each of two geographic regions: north of Acapulco and from Acapulco southward. Stations within the northern region are marginally correlated with the Peru stations and lag the latter by several months. Associated with this, the sea level anomalies at the California stations lead the (local) shore temperature anomalies by 2–6 months at low (interannual) frequencies.

c. *Wind stress*

The time series of monthly alongshore wind stress anomalies along the Pacific coast of North America are characterized by two macroenvironments (Fig. 4c). To the north, from Neah Bay (48°N) to Yakutat (59°N), the largest anomalies occur during the winter months and the variance increases monotonically with increasing latitude (Fig. 2; Table 2). To the south, from Crescent City (42°N) to Mazatlan (23°S), the anomaly variance is invariant with latitude and more independent of season. The northern

assemblage is located within the mid- to high-latitude domain of the atmospheric low pressure systems typical of winter months and the southern stations are influenced by weather patterns in the region of the semipermanent subtropical high of the northeast Pacific. The large positive and negative departures from normal wind stress values depend on the nature and intensity of meteorological activity over these regions. For example, the large positive departures in the Gulf of Alaska are probably related to strong cyclogenesis.

The autocorrelations for the wind stress anomalies (not shown) fall off much more rapidly than those for sea level and shore temperature (Fig. 5). Integral time scales of the stress anomalies (Table 3) are essentially below the limit of resolution for monthly data (one month) in the Gulf of Alaska. They increase at Neah Bay and Crescent City and remain near about two months farther south.

The cross correlations between time series of stress anomaly (not shown) are maximum for neighboring stations in the Gulf of Alaska (0.9) and from San Francisco to San Diego (0.8); the correlations are smaller for neighboring stations in the transitional region from Neah Bay to San Francisco (0.6). The correlation decreases with increasing station separation and falls below the 95% significance level (0.12) between the core regions of the two macroenvironments (Gulf of Alaska and south of Crescent City).

5. Mechanisms for the large-scale coherence of sea level

a. Wave propagation processes

Wyrtki (1975) has suggested that anomalous weakening of easterly winds in the mid and western equatorial Pacific is related to the occurrence of El Niño events in the eastern equatorial Pacific. Analytical and numerical models (McCreary, 1976; Hurlburt *et al.*, 1976; Cane and Sarachik, 1976, 1977) indicate how this mechanism may work through the generation of equatorially trapped baroclinic disturbances and the subsequent propagation of these along the equator in the form of equatorially trapped waves. The response at the eastern boundary to incident equatorially trapped disturbances consists of a reflection in the form of westward propagating baroclinic Rossby waves that are less equatorially confined than the incident disturbance, and a transmission poleward along the boundary in the form of coastal trapped internal Kelvin waves. In general, for an incident disturbance at frequency ω, the response will consist of reflected waves at latitudes with Coriolis parameter f less than a particular f_0 and coastal trapped internal Kelvin waves at latitudes with $f > f_0$ (Cane and Sarachik, 1977). For a two-layer model on a β-plane, $f_0 = \frac{1}{2}\beta c/\omega$, where $\beta = df/dy$ and c is the internal Kelvin wave speed. For low frequency (e.g., interannual), the response consists primarily of reflected waves, but the nature of the reflection is such that variations in equatorial disturbances appear to propagate poleward along the eastern boundary with some of the characteristics of an internal Kelvin wave (Cane and Sarachik, 1977).

An internal Kelvin wave in an idealized two-layer model with a vertical side wall, an upper layer depth of 100 m, and a density difference between layers of $\sigma_t = 1.5$ would propagate at $\sim$100 km day^{-1} independent of frequency or latitude. There is some observational evidence for the poleward propagation of baroclinic disturbances at periods of 4–20 days along the Peru coast. Smith (1978) found a persistent poleward propagation of fluctuations in currents and sea level between 10 and 15°S during 1976 and 1977. The velocity fluctuations are baroclinic over the continental slope and the propagation appears to be nondispersive with a wave speed of $\sim$200 km day^{-1}. These features are generally consistent with those of a coastally trapped internal Kelvin wave which would undoubtedly be modified to some extent by the bottom topography of the continental margin.

The structure of sea level anomalies along the eastern boundaries found here suggests that some sort of wave propagation process may be involved in a spreading of disturbances poleward from the equator. Not only might this account for the considerable alongshore coherence, but also for the small but consistent lags observed along the coast of North America (Fig. 9a). We examined the lagged correlation structure of the sea level anomalies to see if it is consistent with alongshore wave propagation. Of all possible station pairs (171) we eliminated those where the stations were of different hemispheres (65) or less than 20 years of common record existed (20). All of the remaining station pairs (86) were correlated at or above the 95% level of significance and 36 pairs had their maximum correlation at nonzero lags. Of the latter, all occurred in the Northern Hemisphere and in all but three cases the more northern station lagged the more southern one, consistent with poleward propagation.

For each case the phase speed was estimated as the ratio of alongshore station separation to the corresponding lag and was considered to be positive in the poleward sense. The phase speeds are plotted against the magnitudes of the observed lags in Fig. 11. The four poleward, 2-month lags were for the four northernmost stations correlated with Balboa. Most of the 1-month lags (21) were for the nine northernmost stations correlated with Acapulco, San Jose, Balboa and Buenaventura. The remaining 1-month lags (9) were for station pairs within each of those subgroups. The distribution of cases

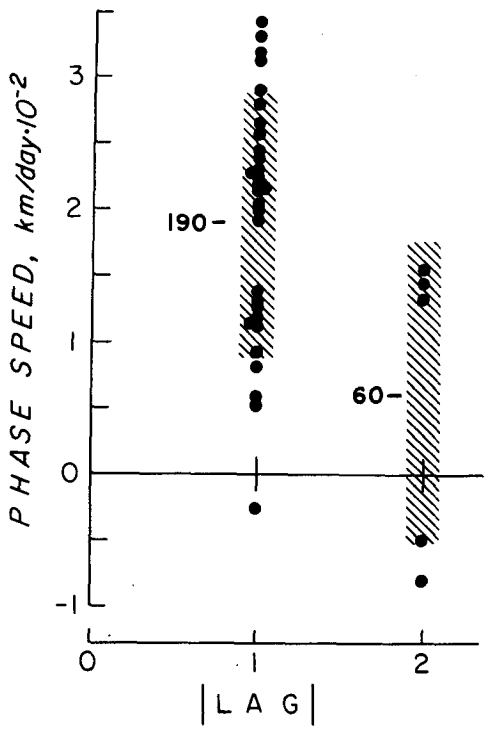

FIG. 11. Distribution of phase speeds computed from maximum lagged cross correlations between sea level stations for non-zero lags, arranged according to the absolute value of the lag used. Positive (negative) phase speeds correspond to poleward (equatorward) propagation. The means are indicated by numbers and the standard deviation ranges by shading.

by lag is significantly skewed toward lags in the poleward sense rather than what might be expected from a zero-lag (simultaneous) relationship or from a random (insignificant) scattering of lags. The overall mean phase speed computed for all 36 cases of non-zero lag was 180 km day^{-1}, within a 95% confidence interval of $\pm$30 km day^{-1}, and a standard deviation of $\pm$100 km day^{-1}.

We also quantified the propagation of sea level fluctuations using 78 phase spectra between the sea level records for which the distribution of sea level coherence in Fig. 7 was constructed. (This includes station pairs from both hemispheres.) All phase lags in the interannual band (2–5 years) corresponding to ($\geq$95%) significant coherence between sea level stations were grouped into 2000 km intervals of station separation (Fig. 12). For each 2000 km interval the mean lag is plotted at the mean separation for the interval, along with the corresponding 95% confidence interval. The propagation characteristic is represented by the regression line ($\pm$95%), which was constrained to pass through the origin. It can be seen that sea level records are consistently phased in the sense of poleward propagation with an estimated phase speed of 75 km day^{-1}. Since the phase estimates at higher frequencies tend to be statistically indistinguishable from zero (and the coherence seldom significant), it is probable that the phase speed estimate from the correlation analysis (180 km day^{-1}) is biased toward high values and should be considered an upper limit. Both estimates are too large to be explained by advection over the separations involved, but bracket a reasonable range of propagation speeds for coastal baroclinic waves.

One might inquire as to possible differences between the propagation characteristics in the two hemispheres. For the Northern Hemisphere the correlation and spectral methods both indicate rapid propagation, i.e., 180 and 75 km day^{-1}, respectively. In the Southern Hemisphere the total alongshore distance is much less, the sea level coherence becomes insignificant for separations beyond 2000–3000 km, and relatively few phase estimates are available. All phase lags from the correlation analysis are zero except one, probably because the separations involved are relatively small (i.e., near the lag resolution of monthly data) and high-frequency coherence is more significant (enhancing the phase bias discussed above). Only 23 spectral phases were available at the interannual frequencies and lead to phase speeds in a 95% confidence range of ~35–50 km day^{-1}. Hence, both methods lead to a Southern Hemisphere propagation that is faster than advection, but the results are more ambiguous due to the limitations of the data.

b. Other mechanisms

There are several alternative ways in which the interannual variabilities of sea level at low and high latitudes might be related. The simplest idea is probably that the sea level behavior is a directly forced response to interannual atmospheric disturbances which likewise propagate northward from the equator. To investigate this possibility, lagged cross correlations of sea level atmospheric pressure (SLP) between stations were calculated to check for a lag structure similar to that found in sea level. SLP's were used because of the unavailability of wind stress data south of Mazatlan. In general, for separation distances $\geq$4000 km, the SLP's in the Northern Hemisphere show lags in the opposite sense, i.e., with poleward stations leading those equatorward by one or two months. In addition, the correlations of SLP and sea level at each station are generally low in magnitude from Buenaventura north to Avila. [The correlations of SLP and sea level are higher north of Avila, with variations very similar to those found in Section 6 for wind stress and sea level (see Fig. 14).] Cross spectral analysis of station pairs from Talara to Neah Bay does not reveal an areal coherence in SLP at interannual frequencies that is similar to the structure found for sea level. The SLP anomalies are less frequently coherent in the inter-

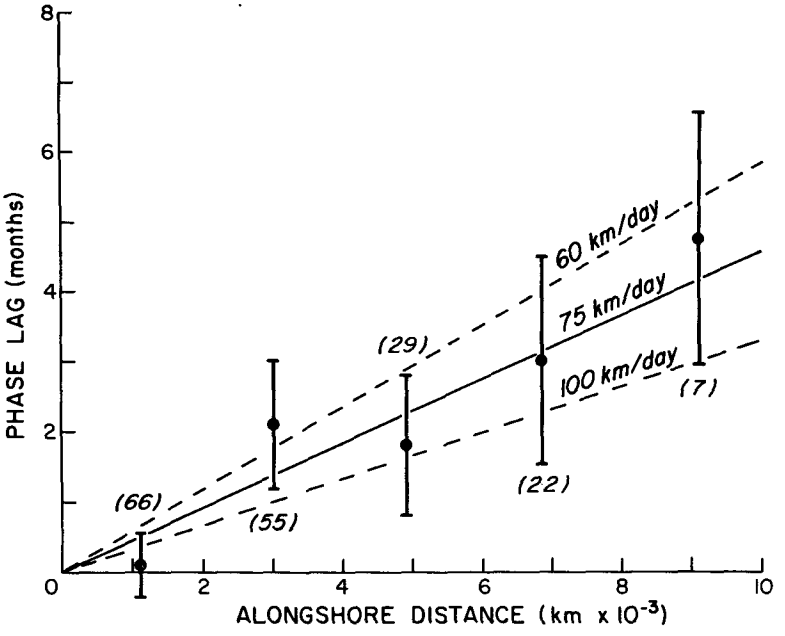

FIG. 12. Distribution of the mean (±95% confidence interval) phase lag between sea level records corresponding to significant (≥95%) coherence estimates in the interannual band (2–5 years) of Fig. 7, shown as a function of station separation and grouped by 2000 km intervals of alongshore distance. The zero-intercept least squares propagation line (solid) and its ±95% confidence interval (dashed) are also shown. The number of observations used in each interval is given in parentheses.

annual band than are sea level anomalies and the lags implied by phase spectra are scattered about equally to either side of zero phase. Moreover, in many cases where one SLP station is coherent with another, one or the other of them (or both) is (are) not locally coherent with sea level. These factors make it seem unlikely that the high coherence and associated phase lags of sea level are the result of direct forcing by the atmosphere.

The other mechanisms are in part dependent on the existence of atmospheric teleconnections between the two regions. The notion of atmospheric teleconnections associated with the Southern Oscillation (and more recently the El Niño occurrences) is based on observations of large-scale atmospheric correlations, especially over the Indo-Pacific region and the Americas. One of the early treatments of the subject was by Walker and Bliss (1932). Perhaps the best known teleconnective mechanism is Bjerknes' (1966) hypothesis that an anomalously warm equatorial ocean will result in an acceleration of the meridional Hadley circulation, causing an increased flux of absolute angular momentum poleward to the (upper level) subtropical jet stream, and farther poleward and downward to the midlatitude (surface) westerlies. He suggested that the westerlies would be strengthened in the longitude sector of the equatorial warming and cited the 1957–58 winter intensification of cyclogenesis in the Gulf of Alaska as an example of this process, in connection with the El Niño conditions in the equatorial Pacific. Rowntree's (1972) numerical experiment reproduced most of the essential features of the North Pacific atmospheric response to equatorial thermal forcing, including the more intense trough in the Gulf of Alaska and the weakened subtropical high pressure cell near 30°N, 130°W. The latter feature in particular was confirmed by the finding of Dorman *et al.* (1974) that sea level pressure at Ship N (30°N, 140°W) tends to decrease during El Niño years.

It may be that at nearly the same time low latitude sea levels rise in response to equatorial forcing, anomalous onshore Ekman transport occurs along the coast of North America due to the alterations of the North Pacific atmosphere through the teleconnective process. Rowntree's (1972) results suggest that about 30 days after the onset of equatorial warming, the mean alongshore wind stress should be more southerly in the range of the Aleutian low and less northerly in the range of the subtropical high. This might produce the sort of behavior we have observed in the sea level anomalies.

To test this hypothesis we correlated the anomalies of shore temperature, sea level, alongshore wind stress and sea level pressure at each station with anomalies of the Southern Oscillation Index (SOI). Our assumption is that the SOI can be used as an index of interannual, equatorial forcing of both the

eastern equatorial Pacific sea level (e.g., Quinn, 1974; Wyrtki, 1975) and the eastern North Pacific atmosphere (e.g., Bjerknes, 1966; Rowntree, 1972). Anomalously low values of the SOI correspond to periods of weakened trade winds and positive anomalies of temperature and sea level in the eastern Pacific.

The latitudinal profiles of the maximum lagged correlations are shown in Fig. 13 along with the corresponding correlation ranges of the 95 and 99% significance levels. The SOI is well correlated with SLP along the Peru coast and marginally correlated with coastal SLP outside of Peru. Shore temperature is correlated above the 99% significance level along the coasts of Peru, Mexico and Central America, and near the 95% level elsewhere. The stress correlations are near the 99% significance level from Crescent City (42°N) to Avila (35°N) and below the 95% level elsewhere. Although the alongshore stress in the Gulf of Alaska was anomalously poleward in the winter of 1957–58 (see Fig. 4c), this apparently is not a pattern that recurs consistently during other low index (El Niño) periods, as it is not reflected in the correlations. The sea level correlations are the highest of all the variables, well above the 99% level of significance from northern Chile to Crescent City, except in the Panama Bight (Balboa and Buenaventura) where the northeast trades may counteract equatorial forcing (see the discussion of Section 4a). The lag structures (not shown) were somewhat erratic but generally consistent with the lag effects discussed in connection with sea level and temperature (Section 4).

A comparison of the time series of sea level and stress anomalies in Fig. 4 and the sea level correlations in Fig. 6a reveals that sea level anomalies along the southern California coast resemble those off Peru more than they do the local stress anomalies, at least on the interannual time scale. The California sea level anomalies are also better correlated with the SOI than are the corresponding stress anomalies (see Fig. 13). These features are inconsistent with what one would expect under the hypothesis of local wind forcing of sea level in response to atmospheric teleconnections. Within the limitations of our data we therefore do not find solid support for this hypothesis as representing the principal mechanism for the large-scale coherence between sea level anomalies of the tropics and the North American coast.

It might be argued that atmospheric teleconnections other than the Hadley circulation are associated with the widespread ocean-atmosphere changes observed on the interannual time scale. Namias (1973) notes that changes in the Northern Hemisphere atmospheric circulation may be a prelude to some of the oceanic phenomena that occur near the equator (e.g., changes in the strength of the North Equatorial Countercurrent). The possibility that such changes might be (nearly) simultaneously related to local wind forcing off North America does

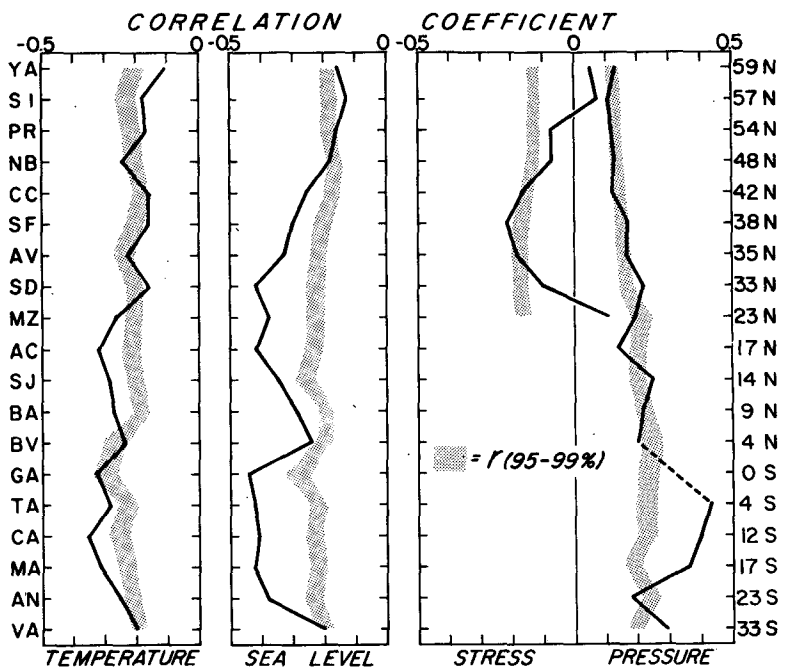

FIG. 13. Latitudinal distribution of the maximum lagged cross correlation (solid lines) between the SOI and (respectively, from left to right) anomalies of shore temperature, sea level, alongshore wind stress and sea level atmospheric pressure. Stippling indicates the 95–99% range of significance.

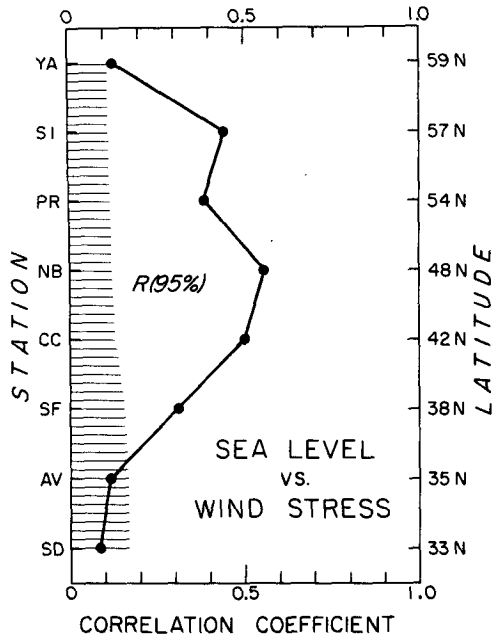

FIG. 14. Latitudinal distribution of the maximum lagged cross correlation between anomalies of sea level and alongshore wind stress at each station. Shading indicates the range for which the significance is less than 95%.

not help to explain the coherence in sea levels, for reasons similar to the above.

Yet another possibility is that an altered atmospheric circulation in the North Pacific might generate surface and subsurface thermal anomalies over much of the eastern North Pacific Ocean. There is considerable evidence that this occurs (e.g., Namias, 1965; Namias and Born, 1970, 1974; White and Walker, 1974; Haney *et al.*, 1978). Such thermal changes would presumably require a longer time, relative to equatorial events and subsequent wave propagation processes, to manifest themselves at North American shore stations in the form of temperature and steric height (sea level) changes. In fact, this mechanism may provide an excellent explanation for the delayed appearance of shore temperature anomalies along the coast of California and Mexico. It is more difficult to see how this accounts for the quasi-simultaneous onset of sea level events along the eastern boundary in both hemispheres. Nor does it explain the tendency for interannual sea level changes to precede similar shore temperature changes by several months in the range of the California Current.

c. *Summary*

Of the various mechanisms we have considered to account for the large-scale coherence of sea level anomalies along the Pacific eastern boundary, the one most consistent with the data is that of poleward propagation by low-frequency, wave dynamical means. Within such a framework, the near-equatorial shore temperature anomalies can perhaps best be understood as slightly lagged (by a month or less) manifestations of the altered thermal structure associated with baroclinic waves. A possibly altered coastal circulation off North America, as suggested by the sea level anomalies, might account (through advection) for temperature changes at lags of several months, as observed. Alternatively, these late-occurring temperature effects may be coastal manifestations of large-scale thermal anomalies in the North Pacific.

6. Relation of sea level and temperature to wind stress

The cross-correlation coefficients between time series of monthly sea level anomalies and corresponding monthly alongshore wind stress anomalies from the same locations are shown in Fig. 14 and given in Table 4. The correlations are positive and reasonably high at the northern stations from Crescent City to Sitka, with the maximum value at Neah Bay. South of Crescent City, the correlations fall off with an intermediate value at San Francisco

TABLE 4. Regressions of anomalies of sea level and shore temperature on the anomalies of alongshore wind stress at each station. Given are the number of paired observations (n), the regression coefficient (b), the (zero lag) correlation coefficient (r), and the correlation coefficient expressed as a multiple of the 95% significance level (r/r_{95}).

	Sea level				Temperature			
Station	n	b	r	r/r_{95}	n	b	r	r/r_{95}
YA	300	0.62	0.124	1.1	300	−0.156	−0.163	−1.5
SI	300	2.85	0.444	3.9	300	0.026	0.025	0.2
PR	300	2.92	0.383	3.3	300	−0.017	−0.013	−0.1
NB	300	8.41	0.557	4.8	300	0.515	0.239	2.0
CC	300	6.29	0.499	3.9	296	0.924	0.350	2.7
SF	300	3.59	0.308	2.0	300	0.340	0.150	1.0
AV	300	1.25	0.115	0.7	300	0.478	0.220	1.3
SD	300	0.86	0.088	0.5	300	0.049	0.024	0.2
MZ	264	2.64	0.146	1.0	240	0.512	0.133	0.9

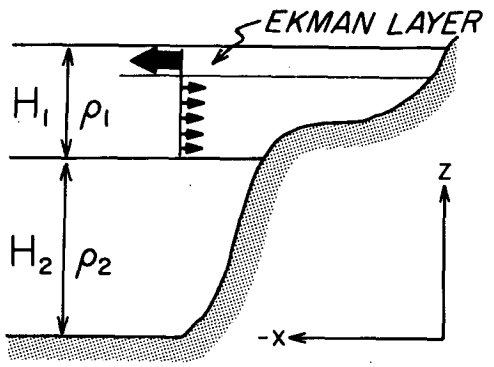

FIG. 15. Schematic of the two-layer model ($\rho_2 > \rho_1$) adjacent to a continental margin, shown for the case of an equatorward wind stress along an eastern ocean boundary.

and very low values at Avila and San Diego. The correlation is also low at the northernmost station, Yakutat. These correlations indicate that there is a response of sea level to the alongshore component of the wind stress from San Francisco north to Sitka. The positive correlations indicate that poleward (equatorward) alongshore stress anomalies are accompanied by an increase (decrease) in sea level. This is consistent with theoretical models of wind-stress-driven coastal currents (e.g., Gill and Schumann, 1974; Gill and Clarke, 1974) and also with the wind stress-sea level correlations found off Oregon during shorter time periods (several months) and for shorter time scales of variability (2–10 days) (e.g., Smith, 1974).

The regression coefficients for sea level on wind stress are given in Table 4. The values increase from San Francisco to Neah Bay, reflecting, in addition to the variation of the correlations, the increase in variance of the sea level anomalies and the relatively uniform variance of wind stress anomalies in this region (Fig. 2). At Prince Rupert and Sitka the regression coefficients are a good deal smaller than at Neah Bay. This reflects the decrease in sea level anomaly variance and the large increase in wind stress anomaly variance north of 48°N (Fig. 2).

South of San Francisco the response of sea level to wind stress is evidently small.[2] It appears that there is a transition at San Francisco from a southern region with relatively little response of sea level to wind stress to a northern region with substantial response. This is consistent with the abrupt increase south of Crescent City (or of San Francisco) of sea level integral time scales (Fig. 5a), of sea level correlation scales (Fig. 6a) and of sea level-Southern Oscillation Index correlations (Fig. 13). It appears that San Francisco may be a dividing point between stations to the south where sea level is influenced by anomalies of equatorial origin and stations to the north where sea level is influenced strongly by local wind stress anomalies.

A possible explanation for the alongshore variation of sea level from Avila to Neah Bay is given below. For that purpose, a simple relation between alongshore sea level slope and the alongshore component of the wind stress is derived here from an idealized model.

We consider the ocean adjacent to an eastern boundary continental margin where for simplicity the stratification is represented by two homogeneous layers of different density (Fig. 15). The alongshore component of the wind stress forces an onshore or offshore Ekman transport of fluid in a surface frictional layer. We assume, on the time scales of interest here, that this mass transport is balanced by an inviscid geostrophic flow in the upper layer normal to the coast. The bottom layer is assumed to be motionless. If the effect of the bottom topography of the continental margin is ignored, this mass balance implies a relation between the wind stress and the alongshore sea level slope. The resulting balance is

$$\zeta_y = \tau/(\rho_1 g H_1), \qquad (6.1)$$

where y is the coordinate along the coast, positive poleward, ζ the sea level height, τ the alongshore component of the wind stress, g the acceleration of gravity, ρ_1 the upper layer water density, H_1 the upper layer depth, and the y subscript denotes partial differentiation.

The relation (6.1) arises on the eastern boundary of most idealized, steady, β-plane ocean circulation models which do not explicitly take into account the effect of the bottom topography of the continental margin (see, e.g., Garvine, 1974). Results from a steady barotropic model of wind-stress-driven shelf flow with sloping topography (Csanady, 1978) indicate that the effects of bottom friction and bottom topography may alter (6.1). It is clear that results from a stratified coastal model which includes the effects of typical continental margin topography and bottom friction would be helpful in interpreting the sea level and stress data here, but an appropriate model of that sort evidently does not exist at present. It has also been suggested (Csanady, 1978) that alongshore pressure gradients on the shelf may be related to the large-scale oceanic circulation. For example, based on results from a numerical model, Beardsley and Winant (1979) have argued that a mean alongshore pressure gradient is imposed on the shelf in the Middle Atlantic Bight by the mean large-scale motion offshore. Effects of this sort might also invalidate (6.1).

We note that Sturges (1974) has attempted to explain north-south alongshore sea level slopes, in the following manner, as being related to the latitudinal

[2] It should be recalled that the coastal wind stress values become less accurate off southern California (Bakun, 1973). The decay of the sea level-wind stress correlations south of Crescent City, however, appears to be more rapid than the decay of validity of the wind stress data is likely to be.

variation of the Coriolis parameter f. Assume for simplicity that the coast is aligned north-south. The alongshore surface velocity v is assumed to be in geostrophic balance, i.e., $fv = g\zeta_x$. An integration of this relation with respect to x over the width L of the coastal current gives

$$\zeta(0) = \zeta(-L) - fg^{-1} \int_0^{-L} v dx, \qquad (6.2)$$

where the coast is at $x = 0$. With the assumptions

$$\zeta_y(-L) = 0, \quad \left(\int_0^{-L} v dx \right)_y = 0, \qquad (6.3a,b)$$

the y derivative of (6.2) yields

$$\zeta_y(0) = f_y g^{-1} \int_0^{-L} v dx, \qquad (6.4)$$

Eq. (6.4) relates $\zeta_y(0)$ to f_y and is essentially the relation used by Sturges (1974) to rationalize alongshore sea level slopes. In fact, although the geostrophic assumption for v is probably good, theoretical models provide no basis for assumptions (6.3a,b) and consequently no support for (6.4). The relation for north-south sea level slope provided by idealized theories is (6.1) (Garvine, 1974).

Since (6.1) is derived from some theoretical models and since it depends primarily on the presumably reasonable assumptions of surface Ekman transport and interior geostrophic onshore flow, it seems worthwhile to test it with the present sea level and wind stress data.

Let the sea level stations be numbered sequentially along the coast with the numbers increasing toward the north. Eq. (6.1) may be integrated in the alongshore direction between two stations m and n ($n > m$) to give

$$\Delta\zeta = \bar{\tau} L_T / (\rho_1 g H_1), \qquad (6.5a)$$

where $\Delta\zeta = \zeta_n - \zeta_m$, L_T is the total alongshore distance between stations m and n, and the integral of τ is approximated by

$$\bar{\tau} L_T = \frac{1}{2} \sum_{i=m}^{n-1} L_{i,i+1}(\tau_i + \tau_{i+1}), \qquad (6.5b)$$

where τ_i is the wind stress at station i, and $L_{i,i+1}$ the alongshore distance between stations i and $i + 1$.

We calculated $\Delta\zeta$ and $\bar{\tau}$ using data from adjacent stations ($n = m + 1$). We next computed the correlation between $\Delta\zeta$ and $\bar{\tau}$ and the regression coefficient of $\Delta\zeta$ on $\bar{\tau}$. Using the known values of L_T, the implied values of the upper layer depths H_1 were found from the regression coefficients. The correlation coefficients are shown in Fig. 16 along with the values computed for H_1 at locations where the correlation is significant at the 95% level. Sea level differences between adjacent stations from Neah Bay to Avila correlated positively and significantly with the averaged wind stress $\bar{\tau}$ in agreement with (6.2). The corresponding values of H_1 in this region are in the range 110–330 m and are in reasonable order-of-magnitude agreement with the depth of the permanent pycnocline. The correlations are low and insignificant to the south, between Avila and San Diego, and to the north, between Neah Bay and Yakutat.

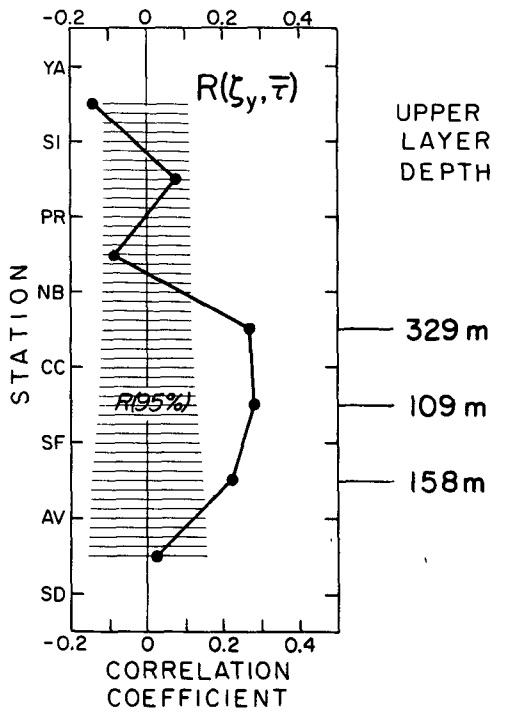

FIG. 16. Latitudinal distribution of the maximum lagged cross correlation between the anomalies of sea level difference and average alongshore wind stress, for adjacent stations. Also given are the upper layer depths estimated by regression for cases where the correlations are significant at the 95% level. Shading indicates the range for which the significance is less than 95%.

These results indicate that the balance (6.2) may be valid to some extent between Neah Bay and Avila. Although the values of the correlation coefficients of $\Delta\zeta$ and $\bar{\tau}$ for the points in this region are not high, the sea level does in fact respond to the wind stress qualitatively in accordance with (6.5). This may be seen more clearly perhaps from an examination of the behavior of the empirical orthogonal functions (EOF's) for the sea level from Neah Bay to Avila. The structure of the first two eigenfunctions and information on the amount of variance explained is given in Table 5. We use a notation such that ϕ_{ij} is the jth component of the ith eigenfunction and $E_i(t)$ is the time series associated with the ith eigenfunction.

The first EOF carries 65% of the total variance and appears to represent the large-scale sea level response, i.e., that which is correlated among these

TABLE 5. Empirical orthogonal functions for sea level from Avila to Neah Bay.

a. First two eigenfunctions (ϕ_{ij})

	Station			
	AV	SF	CC	NB
j =	1	2	3	4
ϕ_{1j}	0.31	0.44	0.56	0.63
ϕ_{2j}	0.73	0.40	−0.09	−0.55

b. Percent of variance explained ($E_i\phi_{ij}$)

	Total	Station			
		AV	SF	CC	NB
	j =	1	2	3	4
$E_1\phi_{1j}$	65	30	62	81	75
$E_2\phi_{2j}$	20	20	15	1	17

stations, to wind stress. The correlation coefficient of the time series $E_1(t)$ associated with the first eigenfunction and the average integrated wind stress $\bar{\tau}$ between Neah Bay and Avila is 0.56, which is relatively high, whereas the correlation of E_2 and $\bar{\tau}$ is 0.17 and relatively low. As shown in Table 5, $E_1\phi_{1j}$ explains most of the sea level variance at the northern three stations, but carries only 30% of the variance at Avila. A large part of the variance at Avila is carried by the second eigenfunction. This again reflects the larger relative influence of wind stress on sea level for stations at and north of San Francisco.

The components of the first eigenfunction ϕ_{1j} are of the same sign and increase monotonically in magnitude in the northward direction. Consequently, the fluctuations in sea level represented by $E_1\phi_{1j}$ are in the same sense at each of the four stations, but increase in magnitude toward the north. This behavior and the high correlation of E_1 with $\bar{\tau}$ is consistent with (6.1) and (6.5). If it is assumed that $E_1\phi_{1j}$ alone represents the total sea level response relevant to (6.1), so that between Neah Bay and Avila $\Delta\zeta = \zeta_4 - \zeta_1 \approx E_1(\phi_{14} - \phi_{11})$, then the correlation of $\Delta\zeta$ and $\bar{\tau}$ is the same as for E_1 and $\bar{\tau}$, 0.56. From the regression coefficient we obtain $H_1 = 383$ m, which again is a reasonable upper layer depth.

The structure of the first eigenfunction ϕ_{1j} is also present in the standard deviations of sea level anomalies which increase in magnitude from San Francisco to Neah Bay (Table 2). It should be noted that this structure does not seem to be simply imposed by a station-to-station variation of the wind stress in a like manner. In contrast to the sea level variations, the standard deviations of the wind stress anomalies remain relatively constant from Avila to Neah Bay (Table 2).

Based on the above results, we conclude that the variation of sea level and wind stress anomalies from Avila to Neah Bay shows some consistency with (6.1) and hence with the presence of a geostrophic baroclinic onshore velocity component which provides a mass balance for the Ekman transport driven by the alongshore component of the stress. This relation does not appear to hold south of Avila or north of Neah Bay. In the southern region, sea level has a small response to wind stress and, as mentioned previously, may well be responding to disturbances which have propagated from lower latitudes. The behavior of sea level north of Neah Bay from Prince Rupert to Yakutat is difficult to explain. The variances of the wind stress anomalies in this region are very large, relative to other regions, but the variances of sea level are similar to those elsewhere (Figs. 2, 4a, 4c). The larger wind stress values are evidently not reflected in higher sea level-stress correlations or in larger magnitudes of the sea level response. The reason for the failure of (6.1) north of Neah Bay is not clear. One possibility is that the effective pycnocline depth H_1 is substantially larger in this region, and that the ζ_y in (6.1) is therefore too small to detect. Another possibility is that the effect of bottom friction on the continental margin has a strong influence on coastal sea level such that (6.1) does not hold at the coast.

It is of interest to inquire if the average seasonal cycles of wind stress and sea level behave consistently with (6.1). A calculation of the average seasonal cycles of $\Delta\zeta$ and $\bar{\tau}$ between Neah Bay and Avila gives two curves which are almost identical in shape with $\bar{\tau}$ leading by one month. Choosing H_1 so that the standard deviations of $\Delta\zeta$ and $\bar{\tau}L_T/(\rho_1 g H_1)$ are equal, we obtain $H_1 = 157$ m. The similarity in shape of the curves and the reasonable value for the H_1 indicate that (6.1) may have some applicability to the average seasonal cycle between Neah Bay and Avila, although the 1-month time lag is not explained. If the predicted mean values of ζ_y for stations between Yakutat and San Diego are calculated from (6.1) using the mean values of the wind stress in Table 2, we find $\zeta_y > 0$ north of Neah Bay and $\zeta_y < 0$ south of Crescent City. This implies that the mean sea level would have a minimum value at some point between Neah Bay and Crescent City where $\zeta_y = 0$. This feature is qualitatively consistent with the variation of steric height along the eastern boundary of the North Pacific calculated by Reid and Mantyla (1976), where a minimum is found somewhat farther south at about 38°N.

The correlation coefficients of monthly shore temperature anomalies with monthly alongshore wind stress anomalies are given in Table 4. These correlations are only significant from Neah Bay to Avila, with the highest correlation at Crescent City. The correlations are positive which implies that poleward (equatorward) alongshore stress anomalies are accompanied by an increase (decrease) in temperature. This sense is consistent with standard

upwelling and downwelling models. It is worth noting that the range of significant correlation, from Neah Bay to Avila, is coincident with the range over which the sea level response was consistent with (6.1). The very small correlations of shore temperature and wind stress north of Neah Bay may be due to local effects influencing the shore temperatures.

7. Summary

We have examined the behavior of the anomalies of monthly mean sea level along the eastern Pacific coast from Yakutat, Alaska to Valparaiso, Chile. The anomalies represent a substantial fraction of the total sea level variability, especially at the Galapagos Islands and along the South American coast, where the seasonal variation of sea level is small. From Antofagasta (23°S) to San Francisco (38°N) the anomaly time series are visually coherent, and they are statistically well correlated from Valparaiso to the Canadian border. Over a similar range there is good correlation of sea level anomalies with the Southern Oscillation Index (SOI) and visually coherent events can be identified that correspond to known occurrences of the El Niño phenomenon. The interannual variability associated with these events appears to contribute greatly to the correlation between widely separated stations (e.g., >3000 km) from Antofagasta to San Francisco. The correlations tend to increase at smaller separations, probably due to the coupling effects of local processes such as regional wind forcing.

A well-defined lagged correlation structure of the sea level anomalies exists which suggests a poleward propagation of events in the northern hemisphere and leads to a phase speed estimate of 180 ± 100 km day^{-1}. Cross-spectral analysis implies that propagation occurs predominantly at subannual frequencies (0.2–0.4 cpy) and leads to a lower range of phase speeds (60–100 km day^{-1}). These estimates are consistent with theory and observations concerning wave propagation processes but are too fast to be explained by large scale advective processes. A similarly persistent lag structure of sea level pressure anomalies, such as might explain the observed sea level structure in terms of an atmospherically forced wave, was not found. Alternative coherence mechanisms can be proposed that link the equatorial and higher latitude anomalies through atmospheric teleconnections, but these seem less plausible since the alongshore wind stress off North America appears much less correlated with the SOI than sea levels are with the SOI or sea levels are among themselves.

The anomalies of monthly shore temperatures are less coherent for large separations and tend to fall into southern and northern modes of variability. The tropical temperature anomalies appear to be mutually coherent and are related to local sea level and to El Niño occurrences. At California stations the temperature anomalies are still related to El Niño occurrences but lag both local sea level and the Peru temperature anomalies by several to many months. The low-latitude fluctuations appear consistent with the coastal upwelling of deepened thermal structures that accompany El Niño events (Wyrtki, 1975). The greatly lagged temperature anomalies along the California coast might be best explained as an advective phenomenon, perhaps associated with atmospheric teleconnections.

The sea level anomaly response to wind stress anomalies undergoes a tenfold increase from San Diego to Neah Bay, while the correlations between the sea level anomalies and the SOI decrease over the same range. These relationships are consistent with the notion that, with increasing latitude, energetic winter storms become more effective in forcing a local response in sea level that masks the freely propagating disturbances originating near the equator. They are also consistent with the converse, i.e., that wind-sea level relationships become more evident as the energy of the equatorial disturbances dissipates with increasing latitude. Between Avila and Neah Bay the relation between the alongshore sea level slope and wind stress shows some consistency with that implied by a baroclinic geostrophic onshore (offshore) flow balancing an offshore (onshore) Ekman transport.

Acknowledgments. This research was supported by National Science Foundation under Grants OCE 78-03382 (for D. B. Enfield) and OCE 78-03380 (for J. S. Allen) as part of the Coastal Upwelling Ecosystems Analysis (CUEA) Program, and also (for J. S. Allen) by National Science Foundation Grants DES 75-15202 and OCE 78-26820. The authors thank A. Huyer, K. Brink and R. L. Smith for helpful comments; they also thank C. Nelson, A. Bakun and S. Pazan for providing data used in this study.

REFERENCES

Bakun, A., 1973: Coastal upwelling indices, west coast of North America, 1946–71. Tech. Rep. NMFS SSRF-671, NOAA, Seattle, WA, 103 pp.

——, 1975: Daily and weekly upwelling indices, west coast of North America, 1967–73. Tech. Rep. NMFS SSRF-693, NOAA, Seattle, WA, 114 pp.

Beardsley, R. C., and C. D. Winant, 1979: On the mean circulation in the Mid-Atlantic Bight. *J. Phys. Oceanogr.*, **9**, 612–619.

Bjerknes, J., 1966: A possible response of the atmospheric Hadley circulation to equatorial anomalies of ocean temperature. *Tellus*, **18**, 820–829.

Bretschneider, D. F., and D. R. McLain, 1976: Anomalies of monthly mean sea level along the west coasts of North and South America. *Marine Fisheries Climate*, Vol. 3, U.S. Dept. of Commerce, 95–102.

Cane, M. A., and E. S. Sarachik, 1976: Forced baroclinic ocean motions: I. The linear equatorial unbounded case. *J. Mar. Res.*, **34**, 629–665.

——, and ——, 1977: Forced baroclinic ocean motions: II. The linear equatorial bounded case. *J. Mar. Res.*, **35**, 395–432.

Csanady, G. T., 1978: The arrested topographic wave. *J. Phys. Oceanogr.*, **8,** 47–62.

Davis, R. E., 1976: Predictability of sea surface temperature and sea level pressure anomalies over the north Pacific Ocean. *J. Phys. Oceanogr.*, **6,** 249–266.

Dorman, C. E., C. A. Paulson and W. H. Quinn, 1974: An analysis of 20 years of meteorological and oceanographic data from ocean station N. *J. Phys. Oceanogr.*, **4,** 645–653.

Forsbergh, E. D., 1969: On the climatology, oceanography and fisheries of the Panama Bight. *Inter-Amer. Trop. Tuna Comm., Bull.*, **14,** 49–385.

Garvine, R. W., 1974: Ocean interiors and coastal upwelling models. *J. Phys. Oceanogr.*, **4,** 121–125.

Gill, A. E., and A. J. Clarke, 1974: Wind-induced upwelling, coastal currents and sea-level changes. *Deep-Sea Res.*, **21,** 325–345.

——, and E. H. Schumann, 1974: The generation of long shelf waves by the wind. *J. Phys. Oceanogr.*, **4,** 83–90.

Haney, R. L., W. S. Shiver and K. H. Hunt, 1978: A dynamical-numerical study of the formation and evolution of large-scale ocean anomalies. *J. Phys. Oceanogr.*, **8,** 952–969.

Hastenrath, S., 1976: Variations in low-latitude circulation and extreme climatic events in the tropical Americas. *J. Atmos. Sci.*, **33,** 202–215.

Hayes, S. P., 1979: Variability of current and bottom pressure across the continental shelf in the northeast Gulf of Alaska. *J. Phys. Oceanogr.*, **9,** 88–103.

——, and J. D. Schumacher, 1976: Description of wind, current and bottom pressure variations on the continental shelf in the northeast Gulf of Alaska from February to May 1975. *J. Geophys. Res.*, **81,** 6611–6419.

Hickey, B. M., 1979: The California Current system—hypotheses and facts. *Progress in Oceanography*, Vol. 8, Pergamon Press, 191–279.

Hurlburt, H. E., J. C. Kindle and J. J. O'Brien, 1976: A numerical simulation of the onset of El Niño. *J. Phys. Oceanogr.*, **6,** 621–631.

Huyer, A., 1977: Seasonal variation in temperature, salinity and density over the continental shelf off Oregon. *Limnol. Oceanogr.*, **22,** 442–453.

——, B. M. Hickey, J. D. Smith, R. L. Smith and R. D. Pillsbury, 1975: Alongshore coherence at low frequencies in currents observed over the continental shelf off Oregon and Washington. *J. Geophys. Res.*, **80,** 3495–3505.

——, J. C. Sobey and R. L. Smith, 1979: The spring transition in currents over the Oregon continental shelf. *J. Geophys. Res.*, **84,** 6995–7011.

Lumley, J. L., and H. A. Panofsky, 1964: *The Structure of Atmospheric Turbulence*. Interscience, 239 pp.

McCreary, J., 1976: Eastern tropical ocean response to changing wind systems: With application to El Niño. *J. Phys. Oceanogr.*, **6,** 632–645.

Moore, D. W., 1968: Planetary-gravity waves in an equatorial ocean. Ph.D. thesis, Harvard University, 207 pp.

Namias, J., 1965: Macroscopic association between mean monthly sea-surface temperature and the overlying winds. *J. Geophys. Res.*, **70,** 2307–2318.

——, 1973: Response of the equatorial countercurrent to the subtropical atmosphere. *Science*, **181,** 1245–1247.

——, and R. M. Born, 1970: Temporal coherence in North Pacific sea surface temperature patterns. *J. Geophys. Res.*, **75,** 5952–5955.

——, and ——, 1974: Further studies of temporal coherence in North Pacific sea surface temperatures. *J. Geophys. Res.*, **79,** 797–798.

Osmer, S. R., and A. Huyer, 1978: Variations in the alongshore correlation of sea level along the west coast of North America. *J. Geophys. Res.*, **83,** 1921–1927.

Quinn, W. H., 1974: Monitoring and predicting El Niño invasions. *J. Appl. Meteor.*, **13,** 825–830.

——, D. O. Zopf, K. S. Short and R. T. W. Kuo Yang, 1978: Historical trends and statistics of the Southern Oscillation, El Niño, and Indonesian droughts. *Fish. Bull.*, **76,** 663–678.

Reid, J. R., and A. W. Mantyla, 1976: The effect of geostrophic flow upon coastal sea elevations in the northern North Pacific Ocean. *J. Geophys. Res.*, **81,** 3100–3110.

Roden, G. I., 1960: On the nonseasonal variations in sea level along the west coast of North America. *J. Geophys. Res.*, **65,** 2809–2826.

——, 1966: Low-frequency sea level oscillations along the Pacific coast of North America. *J. Geophys. Res.*, **71,** 4755–4776.

Rowntree, P. R., 1972: The influence of tropical east Pacific Ocean temperatures on the atmosphere. *Quart. J. Roy. Meteor. Soc.*, **98,** 290–321.

Smith, R. L., 1974: A description of current, wind and sea level variations during coastal upwelling off the Oregon coast, July–August 1972. *J. Geophys. Res.*, **79,** 435–443.

——, 1978: Poleward propagating perturbations in currents and sea levels along the Peru coast. *J. Geophys. Res.*, **83,** 6083–6092.

Sturges, W., 1974: Sea level slope along continental boundaries. *J. Geophys. Res.*, **79,** 825–830.

Walker, G. T., and E. W. Bliss, 1932: World weather V. *Mem. Roy. Meteor. Soc.*, **4,** 53–84.

White, W. B., and A. E. Walker, 1974: Time and depth scales of anomalous subsurface temperature at ocean weather stations P, N and V in the north Pacific. *J. Geophys. Res.*, **79,** 4517–4522.

Wyrtki, K., 1975: El Niño—the dynamic response of the equatorial Pacific Ocean to atmospheric forcing. *J. Phys. Oceanogr.*, **5,** 572–584.

——, 1977: Sea level during the 1972 El Niño. *J. Phys. Oceanogr.*, **7,** 779–787.